Nuclear Physics B115 (1976) 82–113

A STUDY OF K^-n INTERACTIONS IN THE c.m. ENERGY RANGE FROM 1.60 TO 1.75 GeV

V. HEPP
CERN, Geneva

O. BRAUN, H.J. GRIMM *, H. STRÖBELE, C. THÖL and T.J. THOUW
Institut für Hochenergiephysik der Universität Heidelberg

D. CAPPS, F. GANDINI **, C. KIESLING, D.E. PLANE *** and W. WITTEK
Max-Planck-Institut für Physik und Astrophysik, München

Received 14 June 1976

We present results of a K^-d experiment performed with the 81 cm Saclay deuterium bubble chamber which was exposed to a K^- beam at 4 momenta between 680 and 840 MeV/c at the CERN PS. Cross sections were measured for inelastic two- and three-body K^-n reactions on the basis of 5200 events/mb. Resonance production in the three-body reactions is discussed. In addition, differential cross sections and polarisations are presented for inelastic two-body reactions.

1. Introduction

K^-d interactions were studied with the 81 cm Saclay deuterium bubble chamber exposed to a separated K^- beam at the CERN PS. Four K^- momentum settings at 686, 738, 788 and 844 MeV/c were chosen in order to cover a K^-n center of mass energy range from 1600 to 1750 MeV.

In this particular energy region several $I = 0$ and $I = 1$ resonant states are present. Due to the scarcity of $\bar{K}^0p$ and K^-n data which yield direct information on the $I = 1$ amplitudes, many contradictory results of partial-wave analyses have been published in the past [1].

The present experiment was designed to investigate the K^-n interaction in the vicinity of the $\Sigma(1660)$ resonance with high statistical accuracy. The results pre-

* Now at GMD, Bonn.
** Now at IBM, Böblingen.
*** Now at CERN, Geneva.

sented here are based on 5200 events/mb in ~500 000 pictures (75% of the available statistics).

The following channels were studied:

$$K^-d \to \Sigma^-\pi^0 p_s \quad (1)$$

$$K^-d \to \Sigma^0\pi^- p_s \quad (2)$$

$$K^-d \to \Lambda\pi^- p_s \quad (3)$$

$$K^-d \to \Sigma^-\pi^+\pi^- p_s \quad (4)$$

$$K^-d \to \Sigma^+\pi^-\pi^- p_s \quad (5)$$

$$K^-d \to \Lambda\pi^-\pi^0 p_s \quad (6)$$

$$K^-d \to \Sigma^-\pi^0\pi^0 p_s \quad (7)$$

$$K^-d \to \Sigma^0\pi^-\pi^0 p_s \quad (8)$$

$$K^-d \to pK^-\pi^- p_s \quad (9)$$

$$K^-d \to n\bar{K}^0\pi^- p_s \quad (10)$$

$$K^-d \to \Lambda\pi^+\pi^- n_s \quad (11)$$

$$K^-d \to p\bar{K}^0\pi^- n_s\,. \quad (12)$$

The subscript s denotes the spectator nucleon. The channels $K^-d \to K^-d$, K^-pn are under study.

The film was scanned and measured in Heidelberg and München using image-plane digitizers, a PEPR and an HPD. Table 1 gives the number of events per topology processed in the two laboratories. For each topology the corresponding reaction channels are also listed.

In part of the film K^-p interactions in deuterium were studied (e.g. channels (11) and (12)) and compared with measurements in hydrogen.

Some details of the experiment are summarised in table 2.

The paper is divided in 4 parts: in sect. 2 the experimental procedure is described; sect. 3 deals with the method of determining K^- nucleon cross sections from deuterium data. In sects. 4 and 5 the results are presented and discussed.

2. Experimental procedure

2.1. Data processing

The film was scanned twice for the topologies listed in table 1. In about half of the film a proton track was required for the two-prong topologies.

For data processing the modified CERN programs THRESH, GRIND and SLICE

Table 1
Number of events for the various topologies

Topology	No. of events	Possible final states
101 a)	3670	$\underline{\Lambda}\pi^-p$, $\underline{\Lambda}\gamma\pi^-p$, $\underline{\Lambda}\pi^-\pi^0p$
200	132000	K^-d, K^-pn, $\Lambda\pi^-p$, $\Sigma^0\pi^-p$
201	24327	$\underline{\Lambda}\pi^-p$, $\underline{\Lambda}\gamma\pi^-p$, $\underline{\Lambda}\pi^-\pi^0p$, $\underline{\Lambda}\pi^+\pi^-n$ b)
210+	21374	$\Sigma^+\pi^-n$, $\Lambda\pi^-p_D$, $\Sigma^0\pi^-p_D$, K^-p_Dn
210−	16018	$\Sigma^-\pi^0p$, $\Sigma^-\pi^+n$ b), K^-_Dpn, $\Lambda\pi^-_Dp$
300	14796	τ decay, $K^-\pi^-pp$
301	189	$\underline{\Lambda}\pi^+\pi^-\pi^-p$
310+	1376	$\Sigma^+\pi^-\pi^-p$
310−	1707	$\Sigma^-\pi^+\pi^-p$, $K^-\pi^-pp$
400	2241	$\Lambda\pi^+\pi^-\pi^-p$, $K^-\pi^-pp$
401	222	$\underline{\Lambda}\pi^+\pi^-\pi^-p$
410+	2127	$\Sigma^+\pi^-\pi^-p$, $\Sigma^+\pi^+\pi^-\pi^-n$
410−	1719	$\Sigma^-\pi^+\pi^-p$, $\Sigma^-\pi^+\pi^+\pi^-n$
Total	221766	

The topology number is defined as follows: the first digit gives the number of charged secondaries, the second digit the number of charged decays, the third digit the number of neutral decays. The sign indicates the charge of the decaying track. $\underline{\Lambda}$ denotes a Λ with a visible decay; the subscript D indicates a secondary interaction with an unseen spectator proton.
a) The one-prong V^0 topology was scanned in ~15% of the film.
b) These K^-p reactions were measured in ~50% of the film.

were used. In the kinematics program GRIND invisible spectator protons were treated as measured with the starting values for the momentum components $p_x = p_y = p_z/1.37 = 0 \pm 30$ MeV/c.

Up to two remeasurements were performed. Ionisation decisions were made partly automatically with the HPD, partly by visual inspection.

2.2. Losses and corrections

Corrections were necessary to compensate for losses due to strange particles with short projected lengths, small projected decay angles and with decays outside of the fiducial volume. Cut-off criteria were applied and weights were calculated for each event in the usual way. An additional correction factor was introduced to account

Table 2
Experimental parameters

Number of frames analyzed	~500 000
Number of scanned events	~221 000
Effective fiducial volume	5.17×10^3 cm^3
Average magnetic field	20.8 kG
Deuterium density	(0.142 ± 0.005) g/cm^3
Beam settings (momentum at chamber entrance)	686, 738, 788, 844 MeV/c
Beam contamination	~2.5%
Number of beam tracks per frame	~8
Number of τ decays	12 764
Total K^- path length	1200 km
Events/mb	5187

for the following effects:

(i) unmeasurable or unprocessed events;
(ii) neutral V^0 decay modes;
(iii) probability of kinematic fit $< 1\%$;
(iv) hyperon lifetime $> 4.5\tau$ (τ = mean lifetime of hyperon)
(v) Glauber correction.

In table 3 the number of accepted events for reactions (1) to (12), the average weights and the additional correction factors are listed. Also given are the cut-off criteria in projected spectator length l_p, maximum spectator momentum p_n, projected length l_s, and projected hyperon decay angle α.

2.3. Ambiguities and background

Reaction (1) $K^-d \to \Sigma^-\pi^0 p_s$ was found to be frequently ambiguous with $K^-d \to \Sigma^-\pi^+ n_s$, K^-np_s, $\pi^-(\Lambda)p_s$ or $\pi^-(\Sigma^0)p_s$. Most ambiguities were resolved by ionisation decisions and by checking the fitted Σ^- momentum against the observed sagitta. The remaining ambiguous events were attributed to reaction (1). We estimate the contamination of the final sample of reaction (1) to be less than 3%. The measured Σ^- mean lifetime ($\tau_{\Sigma^-} = (1.51 \pm 0.02) \times 10^{-10}$ sec) agrees with the accepted value [2]. The three-body final states of reactions (4), (5) and (9) could always be uniquely identified.

In the V^0 topology reaction (11) $K^-d \to \Lambda\pi^+\pi^- n_s$ was separated from the K^-n channels (2), (3), (6) and (8) by the ionisation of the positive track. $\bar{K}^0$ events (reactions (10) and (12)) were identified by the $K^0_s \to \pi^+\pi^-$ decay mode.

Table 3
Correction factors and cut-off criteria

Reaction	Number of accepted events	Average weight	Additional correction factor	Cut-off criteria a)			
				l_p (cm)	p_n (MeV/c)	l_s (cm)	α (rad)
(1) $K^-n \to \Sigma^-\pi^0$	1429	1.22	1.28	0.15	300	0.25	0.06
(2) $K^-n \to \Sigma^0\pi^-$	1092	1.12	1.88	0.15	300	0.15	
(3) $K^-n \to \Lambda\pi^-$	3079	1.15	1.88	0.15	300	0.15	
(4) $K^-n \to \Sigma^-\pi^+\pi^-$	1128	1.21	1.21		300	0.25	0.06
(5) $K^-n \to \Sigma^+\pi^-\pi^-$	1645	1.38	1.20		300	0.25	0.06
(6) $K^-n \to \Lambda\pi^-\pi^0$	1469	1.10	1.89	0.15	300	0.15	
(7) $K^-n \to \Sigma^-\pi^0\pi^0$	80	1.24	1.27	0.15	250	0.25	0.06
(8) $K^-n \to \Sigma^0\pi^-\pi^0$	147	1.10	1.88	0.15	250	0.15	
(9) $K^-n \to pK^-\pi^-$	948	1.00	1.28		300		
(10) $K^-n \to n\bar{K}^0\pi^-$	63	1.14	3.44	0.15	300	0.15	
(11) $K^-p \to \Lambda\pi^+\pi^-$	3351	1.10	1.85		300	0.15	
(12) $K^-p \to p\bar{K}^0\pi^-$	81	1.13	3.44		300	0.15	

a) l_p denotes the minimum projected length of the spectator proton, p_n the maximum lab momemtum of the spectator particle, l_s the minimum projected length of the strange particle, and α the minimum projected angle between the direction of the strange particle and the direction of the charged decay particle in the lab system.

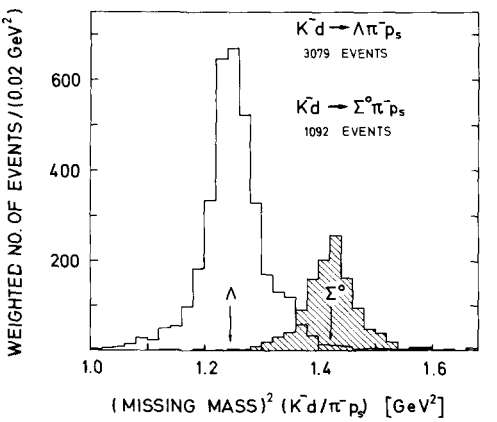

Fig. 1. Distributions of the missing mass squared $MM^2(\pi^-p_s)$ for the events assigned to the reaction $K^-d \to \Lambda\pi^-p_s$ and for the events assigned to the reaction $K^-d \to \Sigma^0\pi^-p_s$ (shaded).

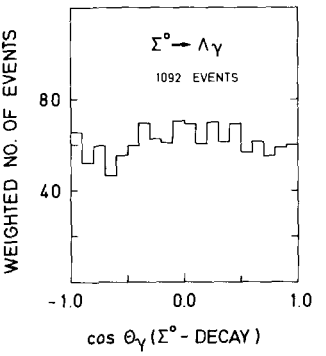

Fig. 2. Polar decay angular distribution for the decay $\Sigma^0 \to \Lambda\gamma$.

Kinematic ambiguities between channels (2), (3), (6) and (8) occurred in about 30% of all V^0 events. No decision is possible on the basis of ionisation. Reactions (2) and (3) were separated by a study of the missing mass $MM(\pi^- p_s)$, missing energy $ME(\Lambda\pi^- p_s)$ and missing momentum $MP(\Lambda\pi^- p_s)$ in the final state. (The particles in parentheses denote those secondaries whose momenta were used to calculate the missing quantity.) The events were attributed to the 4 different channels according to the following criteria:

(i) Ambiguities between $\Lambda\pi^-$ and $\Sigma^0\pi^-$ were resolved in favor of $\Lambda\pi^-$, if $MM^2 + 3 \cdot ME \cdot GeV < 1.54\ GeV^2$ (this relation was found by a study of the MM^2-ME-correlation of the measured events). Otherwise they were considered $\Sigma^0\pi^-$.

(ii) For $K^-n \to \Lambda\pi^-\pi^0$ only unique fits were accepted.

(iii) The missing mass hypothesis (8) was only accepted, if

$$MM^2 - 3\Delta(MM^2) > m_{\pi^0}^2 \ , \quad \text{where} \quad MM^2 = MM^2(\Lambda\pi^- p_s) \, .$$

Fig. 1 shows the distributions of the missing mass $MM^2(\pi^- p_s)$ for all accepted events of channel (3) and (shaded) of channel (2). The purity of the final $\Sigma^0\pi^-$ sample can be checked by the shaded distribution which is centered around the Σ^0 mass. In addition the decay angular distribution for $\Sigma^0 \to \Lambda\gamma$ agrees well with isotropy, as shown in fig. 2. The Λ mean lifetime measured in channels (2), (3) and (6) separately, is consistent with the world average [2]. We find $\tau_\Lambda = (2.55 \pm 0.04) \times 10^{-10}$ sec, $(2.57 \pm 0.06) \cdot 10^{-10}$ sec and $(2.57 \pm 0.05) \cdot 10^{-10}$ sec for the three channels respectively.

3. Determination of cross sections

3.1. Treatment of the deuteron

The spectator momentum distribution was assumed to be described by a deuteron wave function as derived by Reid [3] using soft-core potentials and taking D-wave

admixtures into account. This Hulthén-type distribution was parametrized as a multi-Gaussian [4]. The mass of the interacting nucleon was taken to be off-shell and the mass of the spectator on-shell.

3.2. Flux determination

The incoming K^- flux was determined by a count of τ decays which were identified by kinematic fitting and ionisation measurements. Hereby most of the background $K^- \to \pi^-\pi^0$, $\pi^0 \to e^+e^-\gamma$ was eliminated. The mutual contamination of τ decays and immediate hyperon decays was checked and found to be negligible.

3.3. Calculation of cross sections

The expected number of events N for a cross section of 1 mb was computed by a Monte-Carlo method in which the assumptions of subsect. 3.1 and the K^- flux as determined by τ decays entered. The momentum spread of the incoming kaons was also taken into account.

For the case of a neutron target the following expression was evaluated [5]:

$$\frac{N}{mb} = \rho_n \frac{c\tau}{Bm_K} \sum_{i=1}^{4} N_\tau^i \int \left\{ p_K \frac{\gamma'_K v'_K}{\gamma_K v_K} \right\}_i \frac{1}{\gamma_n} H(\boldsymbol{p})\, d^3\boldsymbol{p} .$$

Quantities with a prime refer to the neutron rest frame. $H(\boldsymbol{p})$ is the Hulthén distribution. The indices K and n refer to the incoming kaon and neutron, p, γ, v denote momenta, Lorentz factors and velocities. In particular:

$$\gamma_n = E_n/m'_n = (m_D - E_p)/m'_n , \qquad m'^2_n = (m_D - E_p)^2 - p_p^2 .$$

The summation goes over the four K^- momenta characterized by N_τ^i τ decays and the integration goes up to the maximum spectator momentum accepted by the cut-off criteria. The constants are: ρ_n, the target nucleon density; c, the speed of light, m_K, the K^- mass; and B is the $K^- \to \pi^+\pi^-\pi^-$ branching fraction.

The advantage of this approach is that the selection criteria for the spectator nucleon could be directly imposed in the Monte-Carlo calculation. The cut-off in the spectator momentum at 300 MeV/c is necessary in order to reduce the contamination by reactions in which final state interactions have occurred.

Fig. 3 shows the spectator momentum spectrum for $K^-d \to \Lambda\pi^- p_s$, $\Lambda\pi^+\pi^- n_s$ and $\Sigma^-\pi^+\pi^- p_s$. It can be seen that the excess of high momentum "spectators" is of the order of 10–20% and channel dependent.

Fig. 4 displays the calculated number of events per mb as a function of the K^-n center of mass energy E^*. The influence of the cut in the projected length of the spec tator track is also indicated in the figure. Cross sections were determined for each channel by dividing the weighted number of events by the calculated number of events/mb for each c.m. energy bin.

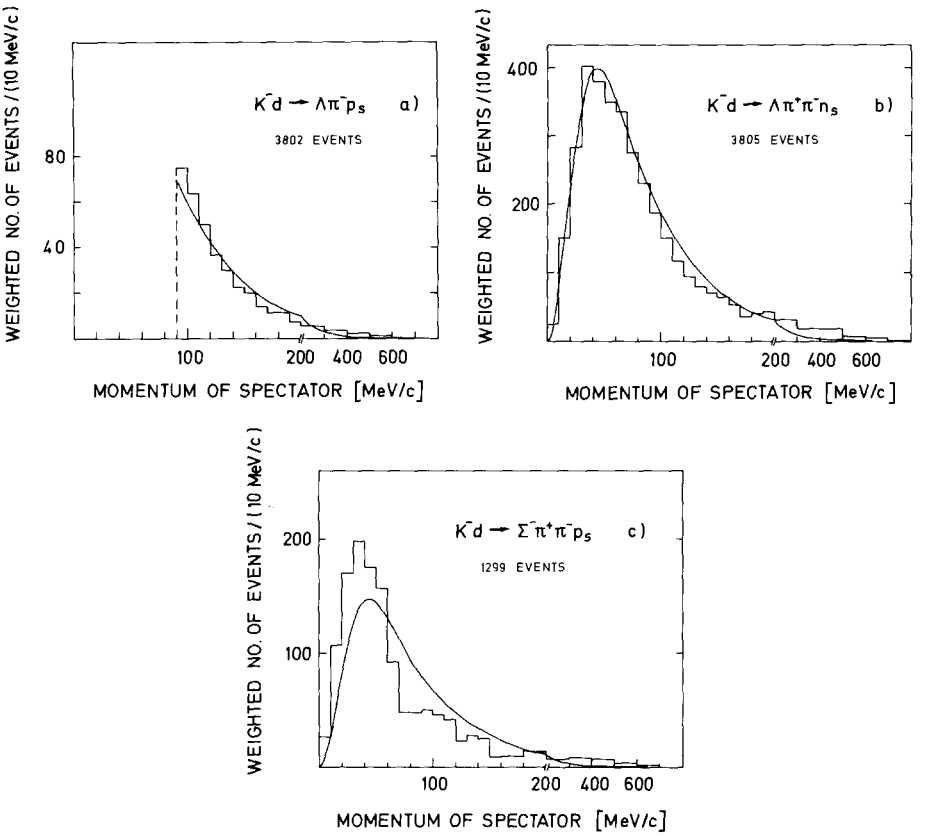

Fig. 3. Momentum distribution for the spectator particle for the reactions: (a) $K^-d \to \Lambda\pi^-p_S$; (b) $K^-d \to \Lambda\pi^+\pi^-n_S$, (c) $K^-d \to \Sigma^-\pi^+\pi^-p_S$. The curves represent the momentum distribution derived from the Reid wave function of the deuteron. The curves are normalized to the number of events below 300 MeV/c.

A factor of 1.07 was introduced to take into account Glauber screening [6]. We hereby assume that the Glauber correction which has been derived for total cross sections is also valid for partial cross sections. In addition, we justify our choice of 7% by comparing the cross sections for reactions (11) and (12) with hydrogen data (see section 4.4).

4. Results

4.1. Two-body reactions

The cross sections for the two-body final states (1) to (3) are given in table 4a and displayed in fig. 5. The cross sections for $\Sigma^-\pi^0$ and $\Sigma^0\pi^-$ are found to be equal, as

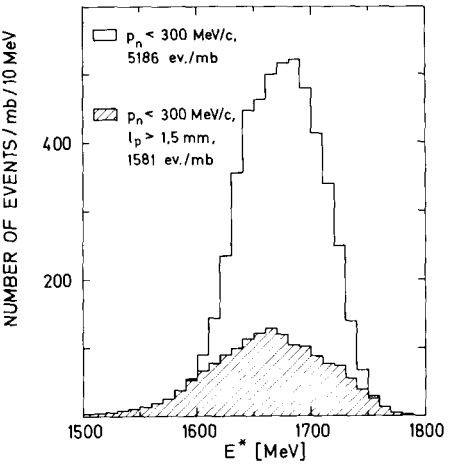

Fig. 4. Expected number of events per mb cross section calculated from the number of observed τ decays with the model described in subsect. 3.3. The spectator momentum has been restricted to values below 300 MeV/c. The shaded distribution corresponds to an additional cut in the projected length of the spectator track: $l_p \geq 1.5$ mm.

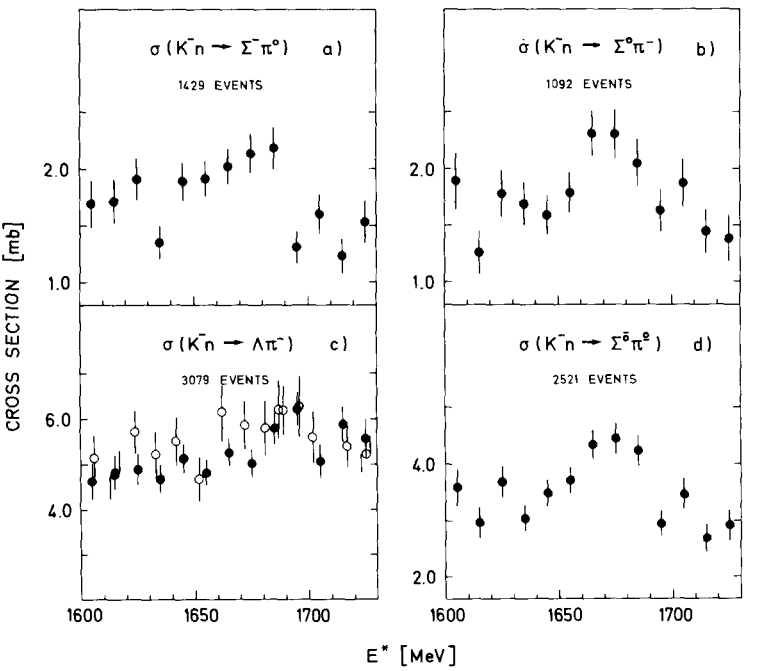

Fig. 5. Cross sections for two-body reactions. In fig. 5c $\sigma(K^-n \to \Lambda\pi^-)$ is compared with $2\sigma(K^-p \to \Lambda\pi^0)$ from ref. [7] (open circles). The points in fig. 5d are the sum of the corresponding points in figs. 5a and 5b.

expected from isospin invariance. The enhancement at ~1675 MeV is due to formation of the $\Sigma(1660)$ resonance which decays predominantly into $\Sigma\pi$ [2]. The summed cross sections of reactions (1) and (2) are given in fig. 5d.

The cross section for $K^-n \to \Lambda\pi^-$ (fig. 5c) is expected to be twice the cross section for $K^-p \to \Lambda\pi^0$ for which representative hydrogen data [7] are also given in the figure. We find satisfactory agreement, both in energy dependence and absolute normalisation. On the average the $\Lambda\pi^-$ cross section is 5.4% smaller than the $\Lambda\pi^0$ cross section multiplied by two.

For the two-body reactions (1) to (3) the differential cross sections were measured. The Σ^0 and Λ polarisations were determined from the Λ decay asymmetry in the usual way. The angular distributions for $\Sigma^-\pi^0$ and $\Sigma^0\pi^-$ were found to be consistent and were combined. In the following the averaged results for the two channels are labelled by $(\Sigma\pi)^-$.

In tables 5 and 6 the differential cross sections $d\sigma/d\Omega$ and polarisations P for $(\Sigma\pi)^-$ and $\Lambda\pi^-$ are given. As usual, $\cos\theta^*$ is defined as the cosine of the meson directions with respect to the incident K^- direction (in the K^-n rest frame).

The A_n and B_n coefficients [8] for $(\Sigma\pi)^-$ and $\Lambda\pi^-$ were determined by the method of moments and are displayed in figs. 6 and 7. Tables 7 and 8 give them in tabular form. In the energy region considered A_n and B_n are compatible with zero for $n \geqslant 7$. The new data on $(\Sigma\pi)^-$ show pronounced structure in the $\Sigma(1660)$ mass region.

Table 4a
Cross sections for two-body reactions

Reaction		$K^-n \to \Sigma^-\pi^0$		$K^-n \to \Sigma^0\pi^-$		$K^-n \to \Sigma^0\bar{\pi}^0$		$K^-n \to \Lambda\pi^-$	
c.m. energy (GeV)	p_{lab}^{eff} a) (GeV/c)	N_{ev}	σ (mb)	N_{ev}	σ (mb)	N_{ev}	σ (mb)	N_{ev}	σ (mb)
1.605	0.596	71	1.70 ± 0.21	59	1.90 ± 0.25	130	3.59 ± 0.32	142	4.63 ± 0.39
1.615	0.618	83	1.71 ± 0.19	45	1.26 ± 0.19	128	2.97 ± 0.27	173	4.83 ± 0.37
1.625	0.640	110	1.91 ± 0.19	76	1.78 ± 0.21	186	3.69 ± 0.28	204	4.90 ± 0.35
1.635	0.662	89	1.36 ± 0.15	83	1.69 ± 0.19	172	3.05 ± 0.24	226	4.69 ± 0.32
1.645	0.683	134	1.89 ± 0.17	86	1.59 ± 0.18	220	3.48 ± 0.24	269	5.15 ± 0.32
1.655	0.705	152	1.91 ± 0.16	104	1.79 ± 0.18	256	3.70 ± 0.24	271	4.81 ± 0.30
1.665	0.726	162	2.02 ± 0.16	139	2.31 ± 0.20	301	4.34 ± 0.26	311	5.26 ± 0.30
1.675	0.748	164	2.14 ± 0.17	132	2.31 ± 0.21	296	4.45 ± 0.27	281	5.03 ± 0.30
1.685	0.769	146	2.18 ± 0.19	104	2.06 ± 0.21	250	4.24 ± 0.28	285	5.80 ± 0.35
1.695	0.790	88	1.32 ± 0.14	80	1.63 ± 0.19	168	2.95 ± 0.23	293	6.22 ± 0.37
1.705	0.812	95	1.60 ± 0.17	80	1.87 ± 0.21	175	3.47 ± 0.27	209	5.07 ± 0.36
1.715	0.833	65	1.23 ± 0.16	57	1.45 ± 0.20	122	2.68 ± 0.25	228	5.89 ± 0.39
1.725	0.854	70	1.53 ± 0.19	47	1.38 ± 0.21	117	2.92 ± 0.28	187	5.58 ± 0.41

a) p_{lab}^{eff} is the kaon lab momentum corresponding to the given c.m. energy assuming an on-shell target nucleon at rest.

Table 4b
Cross sections for three-body reactions

Reaction		$K^-n \to \Sigma^-\pi^+\pi^-$		$K^-n \to \Sigma^+\pi^-\pi^-$		$K^-n \to \Sigma^{\mp}\pi^{\pm}\pi^-$		$K^-n \to \Lambda\pi^-\pi^0$	
c.m. energy (GeV)	p_{lab}^{eff} (GeV/c)	N_{ev}	σ (mb)	N_{ev}	σ (mb)	N_{ev}	σ (mb)	N_{ev}	σ (mb)
1.605	0.596	11	0.18 ± 0.06	16	0.30 ± 0.08	27	0.48 ± 0.10	46	1.53 ± 0.23
1.615	0.618	14	0.14 ± 0.04	30	0.35 ± 0.07	44	0.50 ± 0.08	53	1.45 ± 0.20
1.625	0.640	31	0.20 ± 0.04	47	0.33 ± 0.05	78	0.53 ± 0.06	59	1.38 ± 0.18
1.635	0.662	42	0.17 ± 0.03	89	0.41 ± 0.05	131	0.58 ± 0.06	73	1.46 ± 0.18
1.645	0.683	70	0.23 ± 0.03	113	0.43 ± 0.04	183	0.66 ± 0.05	85	1.60 ± 0.18
1.655	0.705	107	0.33 ± 0.04	109	0.39 ± 0.04	216	0.72 ± 0.05	119	2.04 ± 0.19
1.665	0.726	122	0.35 ± 0.04	157	0.52 ± 0.05	279	0.87 ± 0.06	156	2.57 ± 0.21
1.675	0.748	129	0.37 ± 0.04	179	0.57 ± 0.05	308	0.95 ± 0.06	166	2.84 ± 0.23
1.685	0.769	121	0.34 ± 0.04	213	0.68 ± 0.05	334	1.02 ± 0.06	139	2.74 ± 0.24
1.695	0.790	119	0.36 ± 0.04	204	0.71 ± 0.05	223	1.07 ± 0.06	145	2.91 ± 0.25
1.705	0.812	125	0.44 ± 0.04	181	0.71 ± 0.06	306	1.15 ± 0.07	157	3.58 ± 0.29
1.715	0.833	130	0.56 ± 0.05	170	0.85 ± 0.07	300	1.41 ± 0.09	144	3.64 ± 0.31
1.725	0.854	107	0.65 ± 0.07	137	0.95 ± 0.09	244	1.59 ± 0.11	127	3.67 ± 0.33
		$K^-n \to \Sigma^-\pi^0\pi^0$		$K^-n \to \Sigma^0\pi^-\pi^0$		$K^-n \to pK^-\pi^-$		$K^-n \to n\bar{K}^0\pi^-$	
1.605	0.596	2	0.10 ± 0.07	1	0.03 ± 0.04	2	0.03 ± 0.03		
1.615	0.618			1	0.03 ± 0.04	7	0.06 ± 0.03		
1.625	0.640	6	0.20 ± 0.09	1	0.02 ± 0.03	8	0.04 ± 0.02	1	0.04 ± 0.05
1.635	0.662	4	0.12 ± 0.06	5	0.10 ± 0.05	11	0.04 ± 0.02	1	0.04 ± 0.04
1.645	0.683	5	0.14 ± 0.07	15	0.28 ± 0.08	17	0.05 ± 0.02	1	0.04 ± 0.04
1.655	0.705	10	0.26 ± 0.09	5	0.09 ± 0.04	28	0.08 ± 0.02	2	0.07 ± 0.05
1.665	0.726	14	0.37 ± 0.10	14	0.24 ± 0.07	50	0.13 ± 0.02	4	0.14 ± 0.08
1.675	0.748	6	0.17 ± 0.07	17	0.31 ± 0.08	75	0.19 ± 0.03	6	0.19 ± 0.08
1.685	0.769	4	0.13 ± 0.07	12	0.25 ± 0.08	99	0.25 ± 0.03	4	0.15 ± 0.08
1.695	0.790	10	0.30 ± 0.10	13	0.27 ± 0.08	162	0.43 ± 0.04	11	0.42 ± 0.13
1.705	0.812	9	0.32 ± 0.11	16	0.39 ± 0.10	156	0.48 ± 0.04	7	0.29 ± 0.12
1.715	0.833	8	0.34 ± 0.13	28	0.76 ± 0.15	180	0.68 ± 0.06	11	0.51 ± 0.16
1.725	0.854	2	0.09 ± 0.07	19	0.54 ± 0.13	153	0.82 ± 0.07	15	0.81 ± 0.21

4.2. Three-body reactions

In figs. 8 and 9 and table 4b the cross sections for the three-body channels (4) to (10) are displayed as functions of E^*. The $\Sigma^-\pi^0\pi^0$ and $\Sigma^0\pi^-\pi^0$ final states are underconstrained, but can unambiguously be selected by a missing mass criterion. The background due to other multineutral final states was estimated to be negligible. A study of the overlap of the reactions $K^-d \to \Sigma^0\pi^-\pi^0p$ and $K^-d \to \Lambda\pi^-\pi^0p$ yields an upper limit for the contamination (or loss) of $\Sigma^0\pi^-\pi^0$ by $\Lambda\pi^-\pi^0$ of ~10%.

The $\Sigma^-\pi^+\pi^-$ cross section shows an enhancement around E^* = 1675 MeV, pro-

Table 4c
Cross sections for K^-p reactions

Reaction		$K^-p \to \Lambda\pi^+\pi^-$ a)		$K^-p \to p\bar{K}^0\pi^-$	
c.m. energy (GeV)	p_{lab}^{eff} (GeV/c)	N_{ev}	σ (mb)	N_{ev}	σ (mb)
1.605	0.596	55	2.55 ± 0.35		
1.615	0.618	82	2.30 ± 0.26		
1.625	0.640	133	2.21 ± 0.20	1	0.02 ± 0.02
1.635	0.662	224	2.42 ± 0.17	4	0.04 ± 0.03
1.645	0.683	273	2.44 ± 0.15	5	0.04 ± 0.02
1.655	0.705	313	2.69 ± 0.16	2	0.02 ± 0.02
1.665	0.726	327	2.70 ± 0.15	8	0.07 ± 0.03
1.675	0.748	381	3.18 ± 0.17	5	0.04 ± 0.02
1.685	0.769	428	3.55 ± 0.18	11	0.08 ± 0.03
1.695	0.790	369	3.23 ± 0.17	9	0.07 ± 0.03
1.705	0.812	341	3.46 ± 0.19	14	0.13 ± 0.04
1.715	0.833	248	3.02 ± 0.20	16	0.18 ± 0.05
1.725	0.854	177	2.97 ± 0.23	6	0.10 ± 0.05

a) The events of this reaction were measured only in part of the film.

bably due to the formation of the $\Sigma(1660)$. There is no clear structure in the $\Sigma^+\pi^-\pi^-$ channel. The shoulder around $E^* = 1675$ MeV which can be seen in the $\Lambda\pi^-\pi^0$ cross section is again an indication of the $\Sigma(1660)$ resonance. The cross-section information alone is not sufficient to allow a quantitative determination of the branching fractions $\Sigma(1660) \to \Lambda\pi\pi$, $\Sigma\pi\pi$.

The $pK^-\pi^-$ and $n\bar{K}^0\pi^-$ final states exhibit no structure in the cross sections. The rising trend is probably due to $\Sigma(1765)$ excitation in the upper part of the energy region.

4.3. Resonance production

In the Dalitz plots for $\Sigma^\pm\pi^\mp\pi^-$ strong resonance production of the $\Lambda(1520)$ and, to a lesser extent, also of $\Sigma(1385)$ and/or $\Lambda(1405)$ is seen. The $pK^-\pi^-$ and $n\bar{K}^0\pi^-$ final states are dominated by the $\Lambda(1520)$ and the channel $K^-n \to \Lambda\pi^-\pi^0$ by $\Sigma(1385)$. Thus it appears that the three-body final states are to a large extent "quasi" two-body states formed by a hyperon resonance and a meson [9]. This idea will be pursued in a later study.

Resonance fractions were determined only for channels (4) and (9) in which no crossing resonance bands are present in the Dalitz plots. These final states were fitted to a polynomial background plus a resonance using a Breit-Wigner parametrization with non-relativistic barrier factor.

Table 5a

Differential cross section $\frac{1}{2}[d\sigma/d\Omega\ (K^-n \to \Sigma^-\pi^0) + d\sigma/d\Omega\ (K^-n \to \Sigma^0\pi^-)]$ in mb/sr.

c.m. energy [GeV]

1.605				1.615				1.625			
cos θ*	N_{ev}	dσ/dΩ	Δ dσ/dΩ	cos θ*	N_{ev}	dσ/dΩ	Δ dσ/dΩ	cos θ*	N_{ev}	dσ/dΩ	Δ dσ/dΩ
-0.950	7	0.142	0.048	-0.950	12	0.194	0.048	-0.950	21	0.282	0.054
-0.850	11	0.219	0.060	-0.850	11	0.177	0.046	-0.850	22	0.302	0.055
-0.750	10	0.207	0.058	-0.750	9	0.170	0.041	-0.750	14	0.193	0.044
-0.650	7	0.143	0.048	-0.650	10	0.177	0.043	-0.650	13	0.179	0.042
-0.550	3	0.062	0.032	-0.550	7	0.053	0.018	-0.550	12	0.164	0.041
-0.450	10	0.211	0.058	-0.350	9	0.133	0.041	-0.450	7	0.096	0.031
-0.350	6	0.121	0.045	-0.250	3	0.054	0.024	-0.350	8	0.111	0.033
-0.250	5	0.102	0.041	-0.150	6	0.093	0.034	-0.250	8	0.112	0.033
-0.150	8	0.172	0.052	-0.050	7	0.112	0.036	-0.150	9	0.125	0.035
-0.050	7	0.140	0.048	0.050	7	0.109	0.036	-0.050	2	0.027	0.017
0.050	5	0.105	0.041	0.150	7	0.110	0.036	0.050	10	0.136	0.037
0.150	4	0.087	0.036	0.250	7	0.107	0.036	0.150	9	0.117	0.035
0.250	6	0.126	0.045	0.350	8	0.126	0.039	0.250	6	0.091	0.029
0.350	6	0.123	0.045	0.450	3	0.045	0.024	0.350	5	0.065	0.026
0.450	7	0.147	0.048	0.550	7	0.116	0.036	0.450	8	0.113	0.033
0.550	3	0.063	0.032	0.650	5	0.079	0.031	0.550	8	0.109	0.032
0.650	2	0.043	0.026	0.750	4	0.060	0.028	0.650	6	0.081	0.029
0.750	8	0.173	0.052	0.850	7	0.114	0.036	0.750	11	0.155	0.039
0.850	7	0.147	0.048	0.950	16	0.271	0.055	0.850	13	0.180	0.042
0.950	14	0.317	0.068					0.950	23	0.301	0.053

1.635				1.645				1.655			
cos θ*	N_{ev}	dσ/dΩ	Δ dσ/dΩ	cos θ*	N_{ev}	dσ/dΩ	Δ dσ/dΩ	cos θ*	N_{ev}	dσ/dΩ	Δ dσ/dΩ
-0.950	23	0.288	0.051	-0.950	32	0.329	0.049	-0.950	42	0.402	0.051
-0.850	13	0.157	0.039	-0.850	25	0.259	0.044	-0.850	36	0.335	0.047
-0.750	12	0.158	0.037	-0.750	22	0.226	0.041	-0.750	30	0.286	0.043
-0.650	15	0.180	0.041	-0.650	16	0.160	0.035	-0.650	21	0.193	0.036
-0.550	18	0.219	0.045	-0.550	12	0.120	0.030	-0.550	20	0.179	0.035
-0.450	15	0.175	0.041	-0.450	15	0.152	0.034	-0.450	15	0.137	0.031
-0.350	7	0.081	0.028	-0.350	5	0.055	0.019	-0.350	9	0.080	0.024
-0.250	5	0.060	0.024	-0.250	10	0.099	0.028	-0.250	17	0.152	0.033
-0.150	4	0.049	0.021	-0.150	7	0.068	0.023	-0.150	9	0.084	0.024
-0.050	5	0.062	0.024	-0.050	6	0.059	0.021	-0.050	3	0.027	0.014
0.050	8	0.098	0.030	0.050	7	0.068	0.023	0.050	6	0.056	0.019
0.150	9	0.121	0.032	0.150	7	0.072	0.023	0.150	4	0.037	0.016
0.250	3	0.035	0.019	0.250	4	0.039	0.017	0.250	6	0.054	0.019
0.350	5	0.059	0.024	0.350	7	0.082	0.023	0.350	4	0.038	0.016
0.450	3	0.034	0.018	0.450	8	0.080	0.025	0.450	12	0.109	0.027
0.550	8	0.098	0.030	0.550	9	0.090	0.026	0.550	10	0.094	0.025
0.650	8	0.093	0.030	0.650	9	0.088	0.026	0.650	14	0.129	0.030
0.750	14	0.178	0.040	0.750	13	0.131	0.031	0.750	14	0.133	0.030
0.850	12	0.153	0.037	0.850	26	0.281	0.044	0.850	18	0.171	0.034
0.950	10	0.129	0.033	0.950	29	0.319	0.047	0.950	25	0.249	0.040

1.665				1.675				1.685			
cos θ*	N_{ev}	dσ/dΩ	Δ dσ/dΩ	cos θ*	N_{ev}	dσ/dΩ	Δ dσ/dΩ	cos θ*	N_{ev}	dσ/dΩ	Δ dσ/dΩ
-0.950	58	0.554	0.062	-0.950	48	0.463	0.059	-0.950	39	0.330	0.054
-0.850	44	0.434	0.054	-0.850	47	0.457	0.057	-0.850	38	0.337	0.054
-0.750	24	0.231	0.040	-0.750	36	0.348	0.050	-0.750	30	0.292	0.048
-0.650	35	0.361	0.049	-0.650	25	0.243	0.042	-0.650	29	0.289	0.047
-0.550	12	0.109	0.028	-0.550	21	0.199	0.038	-0.550	18	0.179	0.037
-0.450	16	0.148	0.033	-0.450	17	0.162	0.034	-0.450	12	0.121	0.030
-0.350	10	0.092	0.026	-0.350	13	0.127	0.030	-0.350	7	0.072	0.023
-0.250	6	0.054	0.020	-0.250	6	0.059	0.020	-0.250	3	0.028	0.015
-0.150	7	0.064	0.021	-0.150	11	0.106	0.028	-0.150	5	0.051	0.019
-0.050	6	0.056	0.020	-0.050	8	0.077	0.024	-0.050	2	0.020	0.012
0.050	2	0.020	0.011	0.050	2	0.022	0.012	0.050	12	0.117	0.030
0.150	3	0.029	0.014	0.150	3	0.029	0.014	0.150	7	0.073	0.023
0.250	7	0.069	0.021	0.250	5	0.046	0.019	0.250	13	0.132	0.031
0.350	9	0.085	0.024	0.350	8	0.079	0.024	0.350	14	0.140	0.033
0.450	11	0.105	0.027	0.450	10	0.105	0.026	0.450	13	0.101	0.027
0.550	10	0.099	0.026	0.550	10	0.095	0.026	0.550	11	0.115	0.029
0.650	21	0.201	0.037	0.650	17	0.160	0.034	0.650	17	0.181	0.036
0.750	21	0.202	0.037	0.750	18	0.177	0.035	0.750	28	0.298	0.046
0.850	13	0.232	0.035	0.850	34	0.362	0.049	0.850	19	0.216	0.038
0.950	32	0.325	0.046	0.950	20	0.211	0.037	0.950	14	0.172	0.033

Table 5a (continued).

c.m. energy [GeV]	1.695			1.705			1.715		
cos θ*	N_{ev}	dσ/dΩ	Δ dσ/dΩ	cos θ*	N_{ev}	dσ/dΩ	Δ dσ/dΩ	cos θ*	N_{ev}	dσ/dΩ	Δ dσ/dΩ
-0.950	32	0.348	0.054	-0.950	31	0.413	0.064	-0.950	21	0.226	0.155
-0.850	17	0.195	0.039	-0.850	27	0.342	0.059	-0.850	16	0.224	0.048
-0.750	17	0.178	0.033	-0.750	19	0.258	0.050	-0.750	8	0.111	0.034
-0.650	18	0.191	0.040	-0.650	12	0.165	0.043	-0.650	10	0.138	0.038
-0.550	7	0.074	0.025	-0.550	8	0.106	0.032	-0.550	5	0.069	0.027
-0.450	6	0.072	0.023	-0.450	6	0.077	0.028	-0.450	7	0.102	0.032
-0.350	7	0.081	0.025	-0.350	10	0.133	0.036	-0.350	4	0.054	0.024
-0.250	3	0.032	0.016	-0.250	5	0.066	0.026	-0.250	7	0.092	0.032
-0.150	8	0.092	0.027	-0.150	3	0.037	0.020	-0.150	3	0.042	0.021
-0.050	4	0.042	0.019	-0.050	4	0.051	0.023	-0.050	4	0.061	0.024
0.100	4	0.022	0.010	0.050	2	0.026	0.016	0.050	2	0.027	0.017
0.250	14	0.155	0.036	0.150	4	0.057	0.023	0.250	12	0.083	0.021
0.350	3	0.088	0.027	0.250	9	0.115	0.034	0.350	5	0.070	0.027
0.450	4	0.044	0.019	0.350	11	0.143	0.033	0.450	8	0.110	0.034
0.550	7	0.082	0.025	0.450	10	0.134	0.036	0.550	15	0.215	0.047
0.650	14	0.160	0.036	0.550	16	0.212	0.046	0.650	8	0.117	0.034
0.750	14	0.157	0.036	0.650	9	0.122	0.034	0.750	9	0.138	0.036
0.850	17	0.200	0.038	0.750	7	0.096	0.030	0.850	5	0.071	0.027
0.950	10	0.119	0.030	0.850	8	0.122	0.032	0.950	2	0.030	0.017
				0.950	6	0.086	0.028				

	1.725		
cos θ*	N_{ev}	dσ/dΩ	Δ dσ/dΩ
-0.938	10	0.262	0.052
-0.813	14	0.187	0.045
-0.688	12	0.160	0.042
-0.563	5	0.067	0.027
-0.438	5	0.067	0.027
-0.250	6	0.047	0.015
0.0	4	0.027	0.012
0.188	3	0.041	0.021
0.313	5	0.068	0.027
0.438	10	0.145	0.038
0.563	15	0.215	0.046
0.688	15	0.212	0.046
0.813	12	0.166	0.042
0.938	5	0.081	0.027

No conclusive results on $\Lambda(1405)$ and $\Sigma(1385)$ production were obtained in the $\Sigma^-\pi^+\pi^-$ channel, because the resonance masses are very close and the non-resonant background is appreciable. On the other hand, the $\Lambda(1520)$ is observed with very little background and can therefore be well-determined.

The cross section for $\Lambda(1520)$ production in channels (4) and (9) is displayed in fig. 10. A major part of it may be explained by the large branching fraction of $\Sigma(1765) \rightarrow \Lambda(1520) + \pi$. We observe good agreement with the corresponding cross sections obtained in hydrogen which are also shown in fig. 10.

Fig. 11 illustrates $\Lambda(1520)$ production as seen in the distributions of the invariant mass of $\Sigma^-\pi^+$ in reaction (4), of pK^- in reaction (9), of $\Sigma^0\pi^0$ in reaction (8) and of $n\bar{K}^0$ in reaction (10). As a consistency check of our data the branching ratio $R = \Gamma(\Lambda(1520) \rightarrow \Sigma\pi)/\Gamma(\Lambda(1520) \rightarrow \bar{K}N)$ was evaluated from channels (4) and (9) and compared with the world average. We obtain $R = 0.75 \pm 0.15$ in agreement with $R = 0.85 \pm 0.06$ [2].

Table 5b
Polarisation P for the reaction $K^- n \to \Sigma^0 \pi^-$.

c.m. energy [GeV]

1.605			1.615			1.625		
cos θ*	N_{ev}	P ΔP	cos θ*	N_{ev}	P ΔP	cos θ*	N_{ev}	P ΔP
-0.900	10	-0.360 1.183	-0.900	5	4.301 2.527	-0.900	16	2.028 1.337
-0.700	5	-0.851 2.133	-0.700	3	-2.123 2.203	-0.700	13	0.172 1.565
-0.500	2	0.923 0.443	-0.500	4	1.147 2.625	-0.500	6	1.111 1.532
-0.300	6	-1.219 1.699	-0.300	5	-0.741 3.407	-0.300	7	2.528 1.538
-0.100	5	-1.066 1.639	-0.100	5	-0.216 0.935	-0.100	3	0.998 0.633
0.100	3	1.435 1.279	0.100	4	2.652 1.376	0.100	5	-1.366 1.139
0.300	7	0.786 1.494	0.300	9	2.535 1.476	0.300	5	1.592 2.359
0.500	5	-1.965 1.576	0.500	5	-1.616 1.125	0.500	5	-0.172 2.621
0.700	7	-0.613 2.911	0.700	2	-3.455 2.343	0.700	8	0.452 0.905
0.900	11	2.177 1.124	0.900	10	-1.609 1.244	0.900	15	-0.692 1.120

1.635			1.645			1.655		
cos θ*	N_{ev}	P ΔP	cos θ*	N_{ev}	P ΔP	cos θ*	N_{ev}	P ΔP
-0.900	16	3.156 1.333	-0.900	19	1.493 0.916	-0.900	25	-0.475 0.929
-0.700	12	1.480 1.249	-0.700	15	1.198 1.460	-0.700	20	-0.666 1.033
-0.500	13	-0.387 1.477	-0.500	12	1.309 1.144	-0.500	10	1.396 1.603
-0.300	7	2.883 1.574	-0.300	5	0.546 0.833	-0.300	11	0.383 1.155
-0.100	2	-2.225 1.936	-0.100	5	-1.361 3.144	-0.100	6	0.647 0.261
0.100	4	2.312 1.963	0.100	3	4.177 3.547	0.100	3	6.404 3.882
0.300	5	4.293 3.949	0.300	6	0.249 0.869	0.300	3	-2.063 1.896
0.500	6	2.266 1.594	0.500	10	1.344 1.055	0.500	12	2.309 1.333
0.700	13	-1.040 0.978	0.700	12	-0.732 1.351	0.700	14	1.228 0.935
0.900	13	-0.390 1.302	0.900	19	-0.253 1.049	0.900	25	0.167 0.591

1.665			1.675			1.685		
cos θ*	N_{ev}	P ΔP	cos θ*	N_{ev}	P ΔP	cos θ*	N_{ev}	P ΔP
-0.900	49	1.179 0.635	-0.900	39	-0.578 1.728	-0.900	30	0.342 0.937
-0.700	28	0.531 0.541	-0.700	27	-0.674 0.900	-0.700	23	-0.502 0.914
-0.500	12	-1.017 1.570	-0.500	15	-1.396 1.408	-0.500	12	0.572 0.974
-0.300	8	1.680 1.614	-0.300	4	-2.866 1.616	-0.300	4	-2.853 2.182
-0.100	4	0.820 0.966	-0.100	10	0.210 1.083	-0.100	2	-3.007 3.237
0.100	2	4.832 4.110	0.100	6	-0.083 2.122	0.100	9	-0.616 1.153
0.300	6	2.132 1.540	0.300	8	2.203 1.802	0.300	10	0.763 1.147
0.500	8	0.938 0.607	0.500	20	1.424 1.212	0.500	8	3.160 1.602
0.700	22	1.243 1.045	0.700	24	2.474 0.911	0.700	22	1.281 1.141
0.900	22	1.491 0.911				0.900	14	0.179 0.774

1.695			1.705			1.715		
cos θ*	N_{ev}	P ΔP	cos θ*	N_{ev}	P ΔP	cos θ*	N_{ev}	P ΔP
-0.900	20	1.154 1.087	-0.900	24	-1.023 1.959	-0.900	14	-0.374 1.683
-0.700	14	0.904 1.111	-0.700	12	0.215 0.919	-0.700	10	-0.480 2.160
-0.500	5	-0.271 2.277	-0.500	5	0.615 0.358	-0.500	5	-0.646 0.811
-0.300	1	0.322 1.096	-0.300	3	-2.921 1.885	-0.300	6	-0.876 0.765
-0.100	2	-3.282 4.451	-0.100	5	-3.060 3.586	-0.100	2	0.600 2.293
0.300	10	4.054 1.646	0.100	2	-0.697 1.191	0.100	2	4.886 4.038
0.500	6	-1.749 1.469	0.300	11	1.262 2.071	0.300	7	-0.843 0.561
0.700	16	-0.072 1.128	0.500	16	0.840 0.961	0.500	10	-4.421 1.639
0.900	18	1.140 1.071	0.700	9	0.159 1.343	0.700	7	-0.167 0.683
			0.900	8	1.881 1.472	0.900	6	-1.292 2.003

1.725		
cos θ*	N_{ev}	P ΔP
-0.900	6	-1.781 0.722
-0.700	9	0.643 1.634
-0.500	2	1.333 0.733
-0.300	2	-1.239 0.561
-0.100	3	1.033 2.444
0.300	4	-5.590 2.947
0.500	4	-3.627 1.526
0.700	12	-0.301 0.983
0.900	6	0.261 0.971

Table 6a
Differential cross section $d\sigma/d\Omega$ for the reaction $K^-n \to \Lambda\pi^-$ in mb/sr.

c.m. energy [GeV]

1.635				1.615				1.625			
cos θ*	N_{ev}	dσ/dΩ	Δ dσ/dΩ	cos θ*	N_{ev}	dσ/dΩ	Δ dσ/dΩ	cos θ*	N_{ev}	dσ/dΩ	Δ dσ/dΩ
-0.950	10	0.525	0.137	-0.950	6	0.243	0.089	-0.950	7	0.236	0.080
-0.850	2	0.097	0.061	-0.850	5	0.238	0.091	-0.850	16	0.569	0.123
-0.750	10	0.512	0.137	-0.700	7	0.145	0.048	-0.750	15	0.591	0.117
-0.650	6	0.277	0.106	-0.550	10	0.464	0.115	-0.650	15	0.537	0.117
-0.500	7	0.173	0.057	-0.450	7	0.261	0.086	-0.550	5	0.161	0.067
-0.350	6	0.283	0.106	-0.350	6	0.241	0.089	-0.450	7	0.242	0.080
-0.250	5	0.245	0.107	-0.250	10	0.417	0.115	-0.350	3	0.311	0.090
-0.150	3	0.136	0.075	-0.150	5	0.207	0.091	-0.250	5	0.167	0.067
-0.050	5	0.236	0.087	-0.050	5	0.202	0.081	-0.150	6	0.224	0.074
0.100	4	0.101	0.043	0.050	3	0.116	0.063	-0.050	6	0.209	0.074
0.250	7	0.339	0.114	0.150	3	0.126	0.063	0.100	9	0.148	0.045
0.351	3	0.138	0.075	0.250	8	0.331	0.103	0.250	9	0.267	0.083
0.450	12	0.560	0.150	0.350	7	0.272	0.096	0.350	8	0.097	0.052
0.550	10	0.473	0.137	0.450	13	0.514	0.131	0.450	11	0.369	0.103
0.650	19	0.867	0.188	0.550	14	0.549	0.136	0.550	13	0.430	0.109
0.750	14	0.676	0.162	0.650	6	0.244	0.089	0.650	14	0.457	0.113
0.850	18	0.851	0.193	0.750	25	0.989	0.191	0.750	34	1.142	0.176
0.950	12	0.587	0.150	0.850	21	0.855	0.166	0.850	18	0.612	0.129
				0.950	27	1.115	0.188	0.950	23	0.847	0.144

1.625				1.645				1.655			
cos θ*	N_{ev}	dσ/dΩ	Δ dσ/dΩ	cos θ*	N_{ev}	dσ/dΩ	Δ dσ/dΩ	cos θ*	N_{ev}	dσ/dΩ	Δ dσ/dΩ
-0.950	10	0.525	0.136	-0.950	21	0.606	0.107	-0.950	15	0.341	0.078
-0.850	8	0.219	0.071	-0.850	26	0.663	0.119	-0.850	21	0.521	0.092
-0.750	13	0.396	0.090	-0.750	16	0.405	0.093	-0.750	19	0.414	0.087
-0.650	8	0.223	0.071	-0.650	19	0.516	0.102	-0.650	18	0.420	0.085
-0.550	14	0.438	0.100	-0.550	15	0.364	0.090	-0.550	26	0.594	0.102
-0.450	11	0.289	0.083	-0.450	11	0.285	0.077	-0.450	15	0.382	0.078
-0.350	12	0.344	0.087	-0.350	11	0.282	0.077	-0.350	14	0.323	0.075
-0.250	15	0.407	0.097	-0.250	13	0.328	0.084	-0.250	19	0.435	0.083
-0.150	2	0.055	0.035	-0.150	3	0.076	0.040	-0.150	7	0.162	0.053
-0.050	6	0.164	0.061	-0.050	9	0.227	0.070	-0.050	13	1.221	0.063
0.050	4	0.114	0.050	0.050	8	0.212	0.066	0.050	5	0.109	0.045
0.150	5	0.139	0.056	0.150	5	0.141	0.052	0.150	8	0.177	0.057
0.250	10	0.288	0.079	0.250	7	0.182	0.062	0.250	6	0.133	0.049
0.350	8	0.220	0.071	0.350	9	0.230	0.070	0.350	9	0.196	0.060
0.450	10	0.282	0.089	0.450	18	0.471	0.109	0.450	15	0.332	0.078
0.550	10	0.619	0.103	0.550	19	0.480	0.102	0.550	13	0.293	0.072
0.650	17	0.471	0.103	0.650	21	0.550	0.107	0.650	25	0.559	0.100
0.750	27	0.752	0.130	0.750	24	0.644	0.114	0.750	38	0.837	0.124
0.850	20	0.921	0.135	0.850	33	0.891	0.134	0.850	27	0.666	0.108
0.950	27	0.776	0.130	0.950	22	0.602	0.109	0.950	28	0.741	0.106

1.665				1.675				1.685			
cos θ*	N_{ev}	dσ/dΩ	Δ dσ/dΩ	cos θ*	N_{ev}	dσ/dΩ	Δ dσ/dΩ	cos θ*	N_{ev}	dσ/dΩ	Δ dσ/dΩ
-0.950	25	0.564	0.130	-0.950	36	0.873	0.123	-0.950	49	1.101	0.150
-0.850	27	0.627	0.104	-0.850	35	0.843	0.121	-0.850	26	0.717	0.121
-0.750	20	0.465	0.089	-0.750	25	0.551	0.102	-0.750	17	0.445	0.098
-0.650	27	0.619	0.104	-0.650	19	0.408	0.087	-0.650	17	0.457	0.098
-0.550	13	0.403	0.085	-0.550	17	0.391	0.084	-0.550	14	0.377	0.090
-0.450	25	0.612	0.100	-0.450	15	0.353	0.079	-0.450	4	0.159	0.058
-0.350	16	0.379	0.093	-0.350	9	0.224	0.061	-0.350	14	0.372	0.089
-0.250	9	0.202	0.060	-0.250	6	0.135	0.050	-0.250	5	0.155	0.053
-0.150	13	0.265	0.072	-0.150	9	0.203	0.061	-0.150	8	0.217	0.067
-0.050	7	0.151	0.053	-0.050	5	0.114	0.046	-0.050	9	0.243	0.071
0.050	6	0.137	0.049	0.050	2	0.044	0.029	0.050	4	0.105	0.047
0.150	5	0.111	0.045	0.150	2	0.048	0.029	0.150	4	0.107	0.047
0.250	5	0.113	0.045	0.250	3	0.067	0.035	0.250	3	0.076	0.041
0.350	7	0.151	0.053	0.350	4	0.090	0.041	0.350	9	0.233	0.071
0.450	10	0.217	0.063	0.450	11	0.245	0.068	0.450	7	0.186	0.063
0.550	14	0.308	0.075	0.550	16	0.337	0.079	0.550	8	0.210	0.067
0.650	24	0.531	0.098	0.650	25	0.570	0.102	0.650	26	0.686	0.121
0.750	36	0.808	0.120	0.750	32	0.757	0.116	0.750	31	0.820	0.132
0.850	31	0.710	0.111	0.850	35	0.819	0.121	0.850	51	1.406	0.169
0.950	39	0.890	0.124	0.950	38	0.937	0.126	0.950	41	1.164	0.152

Table 6a (continued).

c.m. energy [GeV]	1.695			1.705			1.715		
cos Θ*	N_{ev}	dσ/dΩ	Δ dσ/dΩ	cos Θ*	N_{ev}	dσ/dΩ	Δ dσ/dΩ	cos Θ*	N_{ev}	dσ/dΩ	Δ dσ/dΩ
-0.950	46	1.433	0.175	-0.950	21	0.766	0.128	-0.950	45	1.537	0.205
-0.850	40	1.230	0.163	-0.850	23	0.835	0.148	-0.850	34	1.105	0.178
-0.750	17	0.478	0.107	-0.750	18	0.548	0.118	-0.750	25	0.869	0.153
-0.650	13	0.537	0.110	-0.650	18	0.626	0.118	-0.650	18	0.625	0.130
-0.550	21	0.623	0.118	-0.550	8	0.253	0.079	-0.550	17	0.578	0.126
-0.450	9	0.260	0.078	-0.450	11	0.354	0.093	-0.450	9	0.323	0.092
-0.350	9	0.266	0.078	-0.350	8	0.247	0.079	-0.350	12	0.397	0.106
-0.250	5	0.145	0.058	-0.250	9	0.292	0.084	-0.250	7	0.257	0.081
-0.150	6	0.170	0.063	-0.150	5	0.152	0.062	-0.150	8	0.271	0.087
-0.050	5	0.141	0.058	-0.050	2	0.065	0.039	-0.050	6	0.208	0.075
0.050	6	0.182	0.063	0.050	2	0.064	0.039	0.100	4	0.069	0.031
0.150	5	0.142	0.058	0.250	2	0.020	0.013	0.250	2	0.080	0.043
0.250	4	0.116	0.052	0.450	9	0.279	0.084	0.400	2	0.034	0.022
0.350	3	0.087	0.045	0.550	7	0.211	0.074	0.550	5	0.167	0.068
0.450	5	0.141	0.058	0.650	12	0.367	0.097	0.650	6	0.207	0.075
0.550	12	0.340	0.090	0.750	20	0.622	0.125	0.750	19	0.651	0.133
0.650	19	0.539	0.114	0.850	29	0.942	0.150	0.850	28	0.970	0.162
0.750	24	0.695	0.127	0.950	35	1.283	0.165	0.950	24	0.814	0.150
0.850	47	1.445	0.177								
0.950	30	0.937	0.142								

	1.725		
cos Θ*	N_{ev}	dσ/dΩ	Δ dσ/dΩ
-0.950	32	1.301	0.207
-0.850	23	0.959	0.175
-0.750	15	0.655	0.141
-0.650	14	0.594	0.137
-0.550	13	0.531	0.132
-0.450	4	0.172	0.073
-0.350	8	0.327	0.103
-0.250	8	0.341	0.103
-0.150	3	0.121	0.063
-0.050	5	0.205	0.092
0.050	4	0.169	0.073
0.250	4	0.055	0.024
0.450	5	0.201	0.092
0.550	5	0.199	0.082
0.650	11	0.445	0.121
0.750	18	0.738	0.155
0.850	19	0.837	0.159
0.950	23	0.927	0.163

4.4. K^-p reactions in deuterium

Reactions (11) and (12) are interactions of the K^- with the proton in the deuteron, where the neutron acts as a spectator. These reactions can be used to check the normalization method outlined in subsect. 3.3.

Fig. 12 shows the result (full circles) and representative hydrogen data (open circles) [7]. The numerical values for the cross sections are listed in table 4c. The agreement is satisfactory. The statistically most significant $\Lambda\pi^+\pi^-$ cross section for example differs from the hydrogen results by less than 9% on the average.

The reaction $K^-d \to \bar{K}^0\pi^- pn$ contains both the K^-n channel (10) and the K^-p channel (12). The separation was made by assuming the slower nucleon to be the spectator. It can be shown that this prescription gives a negligible distortion of the

Table 6b
Polarisation P for the reaction $K^-n \to \Lambda\pi^-$

c.m. energy [GeV]

1.605				1.615				1.625			
cos θ*	N_{ev}	P	ΔP	cos θ*	N_{ev}	P	ΔP	cos θ*	N_{ev}	P	ΔP
-0.900	12	-0.243	0.727	-0.900	11	0.914	0.855	-0.900	23	0.223	0.519
-0.700	16	-0.341	0.736	-0.700	7	1.221	0.911	-0.700	30	-0.495	0.444
-0.500	7	0.129	1.083	-0.500	17	1.333	0.688	-0.500	12	0.284	0.655
-0.300	11	1.238	0.851	-0.300	16	1.734	0.629	-0.300	14	0.272	0.585
-0.100	8	0.489	1.203	-0.100	10	0.615	1.033	-0.100	12	1.206	0.787
0.100	4	3.964	1.933	0.100	6	1.776	0.916	0.100	3	0.567	1.117
0.300	10	0.591	0.852	0.300	15	-0.143	0.549	0.300	12	0.552	0.729
0.500	22	0.637	0.512	0.500	27	0.086	0.464	0.500	24	0.268	0.482
0.700	33	0.353	0.458	0.700	31	-0.607	0.453	0.700	48	0.092	0.432
0.900	30	0.265	0.489	0.900	43	0.205	0.412	0.900	41	-0.807	0.429

1.635				1.645				1.655			
cos θ*	N_{ev}	P	ΔP	cos θ*	N_{ev}	P	ΔP	cos θ*	N_{ev}	P	ΔP
-0.900	26	-0.012	0.483	-0.900	47	0.713	0.407	-0.900	36	0.753	0.492
-0.700	21	1.092	0.483	-0.700	35	-0.134	0.401	-0.700	37	0.592	0.397
-0.500	27	-0.523	0.527	-0.500	26	0.863	0.518	-0.500	41	0.946	0.391
-0.300	27	0.808	0.539	-0.300	24	-0.258	0.553	-0.300	24	0.322	0.579
-0.100	9	0.230	0.984	-0.100	12	1.514	0.596	-0.100	17	-0.391	0.558
0.100	8	-0.326	0.665	0.100	13	0.246	0.851	0.100	13	-0.791	0.870
0.300	18	0.433	0.624	0.300	16	-2.196	0.711	0.300	15	0.076	0.835
0.500	29	0.572	0.462	0.500	37	-0.100	0.438	0.500	28	-0.700	0.476
0.700	44	-0.260	0.395	0.700	45	0.155	0.419	0.700	63	-0.164	0.338
0.900	56	-0.078	0.372	0.900	55	-0.519	0.341	0.900	57	-0.751	0.327

1.665				1.675				1.685			
cos θ*	N_{ev}	P	ΔP	cos θ*	N_{ev}	P	ΔP	cos θ*	N_{ev}	P	ΔP
-0.900	52	0.589	0.356	-0.900	71	0.721	0.329	-0.900	66	0.294	0.318
-0.700	47	0.580	0.376	-0.700	43	0.728	0.404	-0.700	34	1.013	0.376
-0.500	43	0.282	0.366	-0.500	32	0.384	0.449	-0.500	20	0.188	0.608
-0.300	25	0.255	0.456	-0.300	15	-0.116	0.703	-0.300	19	0.115	0.631
-0.100	30	-0.784	0.638	-0.100	14	-0.082	0.686	-0.100	17	0.351	0.503
0.100	11	-1.459	0.556	0.100	4	-0.318	1.572	0.100	8	-1.254	0.898
0.300	12	-1.232	0.599	0.300	7	-0.669	0.844	0.300	12	-1.070	0.642
0.500	24	-1.214	0.483	0.500	26	-0.582	0.389	0.500	15	0.623	0.541
0.700	60	-0.374	0.352	0.700	57	-0.463	0.360	0.700	57	-0.691	0.369
0.900	70	-0.131	0.338	0.900	73	-0.428	0.324	0.900	92	-0.525	0.259

1.695				1.705				1.715			
cos θ*	N_{ev}	P	ΔP	cos θ*	N_{ev}	P	ΔP	cos θ*	N_{ev}	P	ΔP
-0.900	86	0.151	0.276	-0.900	48	0.104	0.379	-0.900	79	0.279	0.321
-0.700	35	1.385	0.492	-0.700	36	-0.405	0.487	-0.700	43	0.460	0.420
-0.500	30	0.785	0.489	-0.500	19	-1.137	0.619	-0.500	26	-0.612	0.544
-0.300	14	-0.162	0.746	-0.300	17	1.323	0.689	-0.300	19	-0.317	0.723
-0.100	11	1.154	0.678	-0.100	7	-0.710	0.781	-0.100	14	0.166	0.650
0.100	11	1.261	0.662	0.100	2	2.423	1.972	0.100	4	-1.248	0.695
0.300	7	-1.963	1.132	0.300	2	-0.096	3.138	0.300	2	-1.350	1.384
0.500	17	-0.127	0.688	0.500	16	-1.362	0.615	0.500	7	-1.333	0.404
0.700	43	-0.383	0.464	0.700	32	-0.261	0.436	0.700	25	-1.594	0.515
0.900	77	-0.279	0.321	0.900	64	-0.018	0.320	0.900	52	-1.096	0.355

1.725			
cos θ*	N_{ev}	P	ΔP
-0.900	55	0.503	0.395
-0.700	29	0.137	0.523
-0.500	17	0.305	0.573
-0.300	16	0.860	0.695
-0.100	8	-0.718	0.658
0.100	4	1.882	0.867
0.300	4	0.473	0.777
0.500	10	-1.115	0.744
0.700	29	-1.436	0.532
0.900	39	-0.525	0.433

Hulthén distribution [11]. Our result for the cross section of the reaction $K^-p \to p\bar{K}^0\pi^-$ is compatible with the low statistics hydrogen data in this energy region.

5. Discussion

5.1. The deuteron target

The measurement of inelastic K^-d interactions, presented here, is statistically much more significant than the other published results in this energy region [5,13].

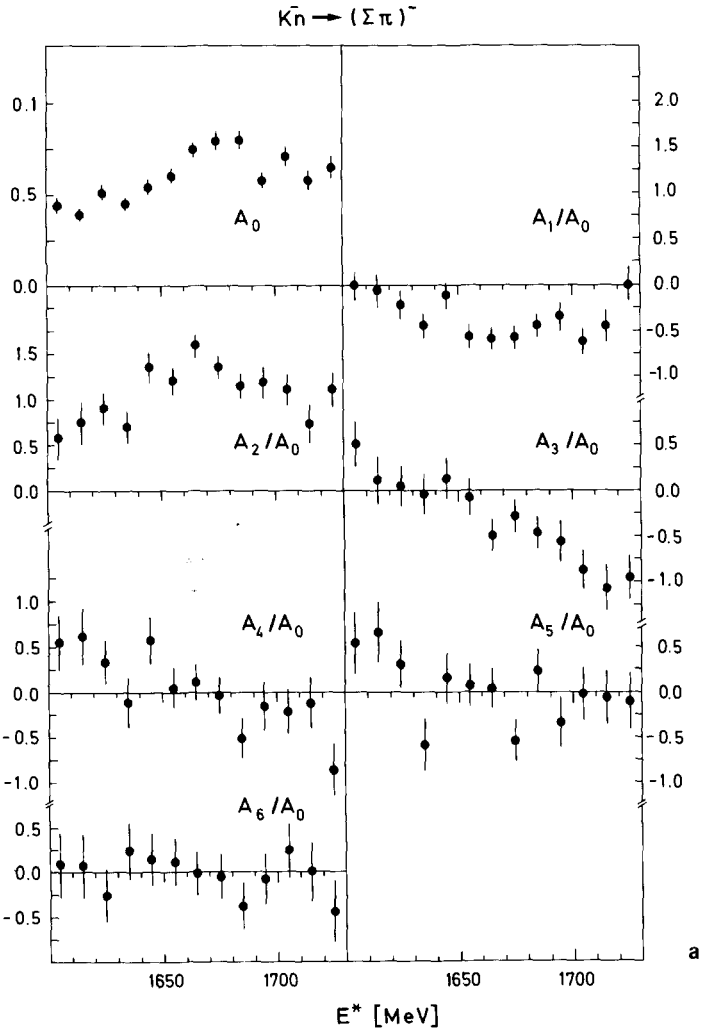

Fig. 6(a). A_0 and A_n/A_0 coefficients ($n \geq 1$) for the reaction $K^-n \to (\Sigma\pi)^-$ (i.e. average between $K^-n \to \Sigma^-\pi^0$ and $K^-n \to \Sigma^0\pi^-$).

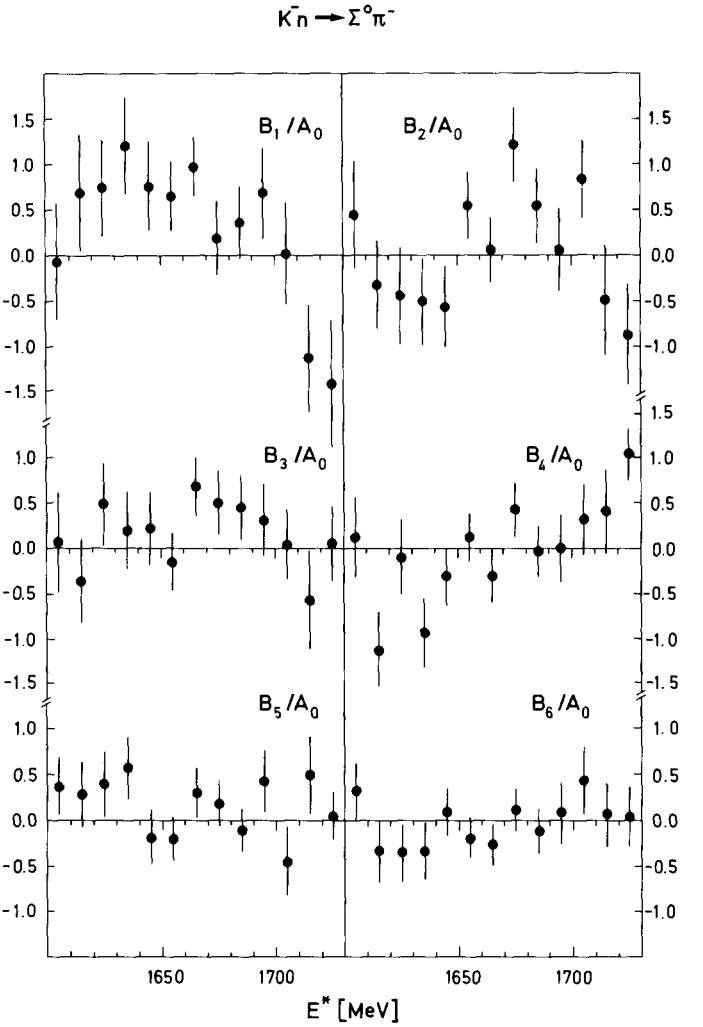

Fig. 6(b). B_n/A_0 coefficients ($n \geq 1$) for the reaction $K^-n \to \Sigma^0\pi^-$.

The problem of systematic errors was very carefully studied, since we extract K^-n reactions from K^-d collisions.

We found no apparent inconsistencies in our data. The results for $K^-d \to \Lambda\pi^+\pi^-n_s$, $p\bar{K}^0\pi^-n_s$ agree well with the corresponding hydrogen measurements *. In addition,

* In a preliminary study of the reactions $K^-d \to \Sigma^-\pi^+n_s$ and $K^-d \to \Sigma^+\pi^-n_s$ good agreement of angular distributions with the corresponding data on free protons is also found. The cross section for $K^-p \to \Sigma^-\pi^+$ as measured in this experiment agrees well with the hydrogen result while the cross section for $K^-p \to \Sigma^+\pi^-$ is about 15% low.

differential cross sections and polarisations for $K^-n \to \Lambda\pi^-$ are in good agreement with $K^-p \to \Lambda\pi^0$, as predicted by isospin invariance (see fig. 7).

We conclude from these observations that the use of the impulse approximation and a screening factor of the order of 7% are justified. The systematic error of the cross sections for K^-n reactions is estimated to be less than 10%. However, we would like to stress that the above argumentation does not exclude the possibility of strong final state interactions in a particular channel.

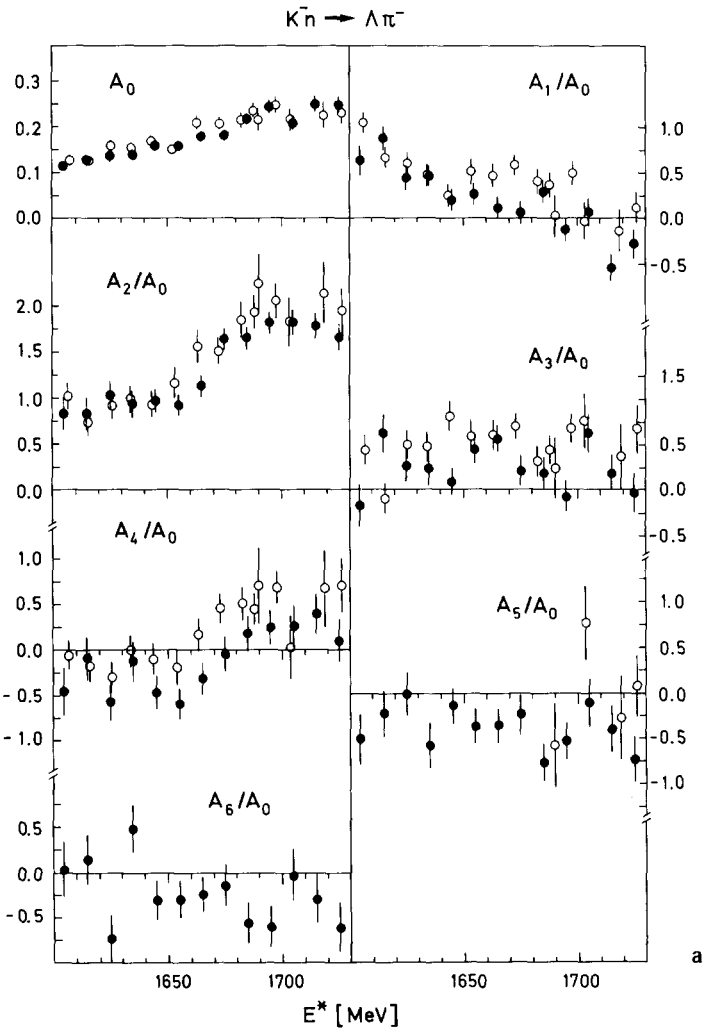

Fig. 7a. A_0, A_n/A_0 coefficients ($n \geq 1$) for the reaction $K^-n \to \Lambda\pi^-$ (full circles). For comparison the corresponding data for the reaction $K^-p \to \Lambda\pi^0$ (open circles) are also shown [7]. For the hydrogen reaction ($2A_0$) is plotted.

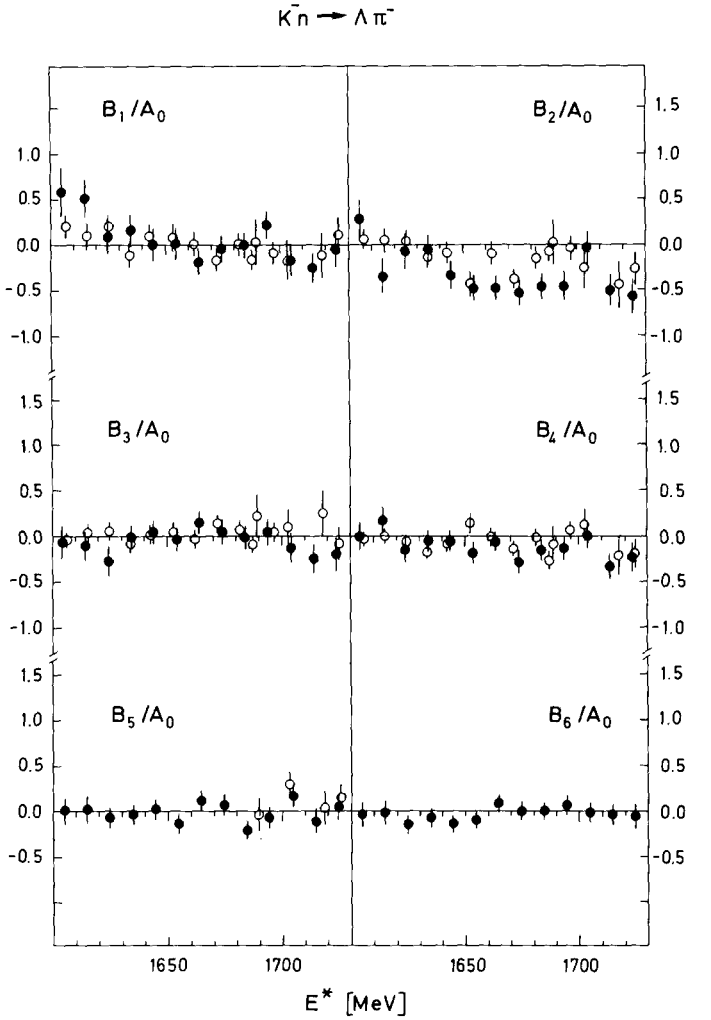

Fig. 7b. B_n/A_0 coefficients ($n \geq 1$) for the reaction $K^-n \to \Lambda\pi^-$ (full circles) in comparison with the corresponding data for the reaction $K^-p \to \Lambda\pi^0$ (open circles) [7].

5.2. The $(\Sigma\pi)^-$ final state

An important result presented in this article is the first high statistics determination of the $I = 1$ $K^-n \to (\Sigma\pi)^-$ cross sections. All published $\Sigma\pi$ partial-wave analyses were hampered by the lack of reliable data on the pure $I = 1$ amplitudes.

Fig. 13a is a compilation of measured and predicted $I = 1$ $\Sigma\pi$ cross sections. The

predicted values were derived from K^-p data using the relation:

$$\tfrac{1}{2}\sigma(\bar{K}N \to \Sigma\pi, I=1) = \sigma(K^-p \to \Sigma^+\pi^-) + \sigma(K^-p \to \Sigma^-\pi^+) - 2\sigma(K^-p \to \Sigma^0\pi^0).$$

The $I = 1$ cross section in this expression is the difference between two large numbers. Furthermore the $\Sigma^0\pi^0$ cross section, which is difficult to measure, is weighted by a factor of 2. The fluctuation of the K^-p predictions is therefore large.

The other source of information on the $I = 1$, $\Sigma\pi$ cross sections is $\bar{K}^0p \to \Sigma^0\pi^+$ data [15–18]. The published results are affected by larger statistical errors than our measurements. They are apparently systematically bigger than $K^-n \to (\Sigma\pi)^-$ data.

Table 7a
A_0 and A_n/A_0 coefficients for the reaction $K^-n \to (\Sigma\pi)^-$.

c.m. energy [GeV]	1.605	1.615	1.625	1.635	1.645	1.655	1.665
A0	0.044	0.039	0.051	0.045	0.054	0.060	0.074
+-	0.004	0.003	0.004	0.003	0.004	0.004	0.004
A1/A0	-0.013	-0.090	-0.230	-0.474	-0.125	-0.582	-0.613
+-	0.168	0.175	0.147	0.145	0.145	0.127	0.123
A2/A0	0.557	0.758	0.908	0.694	1.355	1.199	1.583
+-	0.219	0.223	0.179	0.176	0.164	0.145	0.128
A3/A0	0.507	0.101	0.042	-0.044	0.124	-0.091	-0.500
+-	0.257	0.270	0.216	0.223	0.218	0.193	0.181
A4/A0	0.543	0.619	0.323	-0.118	0.572	0.058	0.115
+-	0.292	0.306	0.231	0.260	0.251	0.212	0.202
A5/A0	0.551	0.672	0.310	-0.582	0.158	0.088	0.041
+-	0.341	0.338	0.258	0.282	0.283	0.239	0.219
A6/A0	0.086	0.074	-0.260	0.254	0.147	0.117	-0.018
+-	0.367	0.360	0.286	0.313	0.306	0.259	0.240

	1.675	1.685	1.695	1.705	1.715	1.725
A0	0.079	0.079	0.057	0.070	0.057	0.064
+-	0.005	0.005	0.004	0.005	0.005	0.006
A1/A0	-0.589	-0.469	-0.361	-0.641	-0.483	0.002
+-	0.120	0.129	0.159	0.149	0.172	0.192
A2/A0	1.343	1.134	1.160	1.087	0.718	1.092
+-	0.131	0.136	0.174	0.170	0.209	0.188
A3/A0	-0.287	-0.466	-0.562	-0.862	-1.076	-0.959
+-	0.177	0.175	0.225	0.219	0.240	0.232
A4/A0	-0.036	-0.506	-0.165	-0.211	-0.119	-0.854
+-	0.201	0.209	0.257	0.245	0.276	0.275
A5/A0	-0.527	0.241	-0.323	-0.009	-0.047	-0.087
+-	0.227	0.236	0.278	0.277	0.308	0.310
A6/A0	-0.055	-0.385	-0.077	0.239	0.004	-0.443
+-	0.256	0.248	0.275	0.299	0.344	0.336

Table 7b
B_n/A_0 coefficients for the reaction $K^-n \to \Sigma^0\pi^-$.

c.m. energy [GeV]	1.605	1.615	1.625	1.635	1.645	1.655	1.665
B1/A0	-0.077	0.684	0.752	1.221	0.755	0.648	0.973
+-	0.635	0.649	0.520	0.544	0.475	0.383	0.329
B2/A0	0.434	-0.329	-0.458	-0.515	-0.579	0.532	0.060
+-	0.592	0.498	0.530	0.463	0.443	0.366	0.353
B3/A0	0.069	-0.360	0.486	0.209	0.228	-0.157	0.696
+-	0.538	0.454	0.456	0.420	0.393	0.310	0.309
B4/A0	0.106	-1.136	-0.106	-0.940	-0.314	0.124	-0.310
+-	0.428	0.422	0.414	0.389	0.308	0.272	0.294
B5/A0	0.362	0.286	0.386	0.592	-0.184	-0.200	0.317
+-	0.325	0.371	0.346	0.341	0.289	0.239	0.266
B6/A0	0.317	-0.323	-0.356	-0.333	0.101	-0.206	-0.265
+-	0.310	0.325	0.321	0.323	0.265	0.214	0.235

	1.675	1.685	1.695	1.705	1.715	1.725
B1/A0	0.196	0.360	0.679	0.008	-1.138	-1.404
+-	0.401	0.394	0.481	0.549	0.574	0.686
B2/A0	1.193	0.534	0.060	0.827	-0.494	-0.876
+-	0.401	0.406	0.453	0.428	0.605	0.540
B3/A0	0.507	0.457	0.310	0.036	-0.569	0.064
+-	0.348	0.354	0.395	0.383	0.541	0.409
B4/A0	0.412	-0.036	0.006	0.315	0.402	1.024
+-	0.286	0.276	0.358	0.383	0.464	0.288
B5/A0	0.186	-0.106	0.432	-0.441	0.515	0.060
+-	0.252	0.229	0.332	0.363	0.431	0.256
B6/A0	0.095	-0.128	0.070	0.423	0.056	0.034
+-	0.229	0.237	0.331	0.358	0.358	0.326

The only other result on the latter channel [12] is in very good agreement with this experiment.

In fig. 13b the measurements of $K^-p \to \Sigma^0\pi^0$ ($I = 0$) are compared with the predictions from K^-n or $\bar{K}^0p$ data. The predicted values were obtained *via* the relations:

$$\sigma(\bar{K}N \to \Sigma\pi, I=0) = 3\sigma(K^-p \to \Sigma^+\pi^-) + 3\sigma(K^-p \to \Sigma^-\pi^+)$$
$$- \tfrac{3}{2}\sigma(K^-n \to \Sigma^-\pi^0) - \tfrac{3}{2}\sigma(K^-n \to \Sigma^0\pi^-),$$

or

$$\sigma(\bar{K}N \to \Sigma\pi, I=0) = 3\sigma(K^-p \to \Sigma^+\pi^-) + 3\sigma(K^-p \to \Sigma^-\pi^+)$$
$$- 3\sigma(\bar{K}^0p \to \Sigma^0\pi^+).$$

The internal consistency of the data in fig. 13b is bad indicating an underestima-

tion of systematic errors. We have not included in fig. 13b the direct measurements of $K^-p \to \Sigma^0\pi^0$ from heavy liquid bubble chamber experiments [20, 21] since they are inconsistent with one another.

5.3. Three-body final states

The cross sections for $K^-n \to \Sigma\pi\pi$, $\Lambda\pi\pi$ show formation of the $\Sigma(1660)$ (fig. 8). Strong intermediate resonance production is observed in all three-body final states, suggesting a quasi two-body analysis. In the $\Sigma\pi\pi$ final state no isospin predictions for pure isospin states can be made which are model independent. The $I = 0$ $\bar{K}N \to \Lambda\pi\pi$

Table 8a
A_0 and A_n/A_0 coefficients for the reaction $K^-n \to \Lambda\pi^-$.

c.m. energy [GeV]	1.605	1.615	1.625	1.635	1.645	1.655	1.665
A0	0.114	0.126	0.136	0.137	0.155	0.156	0.179
+-	0.010	0.010	0.010	0.009	0.010	0.009	0.010
A1/A0	0.616	0.861	0.431	0.453	0.183	0.260	0.113
+-	0.154	0.131	0.134	0.122	0.115	0.110	0.109
A2/A0	0.822	0.821	1.031	0.938	0.960	0.913	1.121
+-	0.178	0.169	0.143	0.141	0.124	0.118	0.116
A3/A0	-0.197	0.602	0.252	0.212	0.074	0.431	0.548
+-	0.228	0.210	0.175	0.188	0.157	0.148	0.148
A4/A0	-0.451	-0.085	-0.579	-0.128	-0.480	-0.606	-0.328
+-	0.258	0.229	0.205	0.216	0.173	0.168	0.168
A5/A0	-0.515	-0.220	-0.013	-0.582	-0.142	-0.378	-0.361
+-	0.285	0.250	0.242	0.246	0.192	0.189	0.183
A6/A0	0.033	0.140	-0.734	0.477	-0.303	-0.290	-0.235
+-	0.303	0.273	0.248	0.266	0.215	0.208	0.195

	1.675	1.685	1.695	1.705	1.715	1.725
A0	0.179	0.216	0.242	0.206	0.249	0.245
+-	0.011	0.013	0.014	0.014	0.016	0.018
A1/A0	0.058	0.288	-0.130	0.064	-0.537	-0.285
+-	0.120	0.120	0.125	0.146	0.134	0.153
A2/A0	1.639	1.643	1.804	1.819	1.772	1.658
+-	0.116	0.120	0.119	0.138	0.135	0.150
A3/A0	0.200	0.186	-0.074	0.622	0.187	-0.034
+-	0.169	0.166	0.171	0.205	0.195	0.209
A4/A0	-0.055	0.168	0.235	0.241	0.382	0.079
+-	0.191	0.188	0.186	0.234	0.220	0.229
A5/A0	-0.230	-0.766	-0.524	-0.106	-0.400	-0.734
+-	0.210	0.206	0.195	0.264	0.247	0.247
A6/A0	-0.139	-0.555	-0.591	-0.017	-0.281	-0.605
+-	0.232	0.224	0.222	0.285	0.268	0.273

Table 8b
B_n/A_0 coefficients for the reaction $K^-n \to \Lambda\pi^-$.

c.m. energy [GeV]	1.605	1.615	1.625	1.635	1.645	1.655	1.665
B1/A0	0.579	0.495	0.093	0.165	0.000	0.010	-0.194
+-	0.256	0.213	0.195	0.180	0.171	0.163	0.145
B2/A0	0.287	-0.353	-0.079	-0.063	-0.345	-0.491	-0.476
+-	0.219	0.188	0.185	0.161	0.155	0.145	0.137
B3/A0	-0.072	-0.113	-0.275	-0.016	0.039	-0.032	0.144
+-	0.183	0.162	0.164	0.132	0.129	0.125	0.121
B4/A0	-0.020	0.155	-0.165	-0.061	-0.069	-0.191	-0.067
+-	0.157	0.150	0.129	0.119	0.114	0.109	0.105
B5/A0	-0.002	0.022	-0.079	-0.044	0.018	-0.136	0.108
+-	0.143	0.136	0.109	0.101	0.101	0.097	0.098
B6/A0	-0.034	-0.015	-0.146	-0.072	-0.140	-0.104	0.073
+-	0.136	0.121	0.104	0.096	0.089	0.090	0.092

	1.675	1.685	1.695	1.705	1.715	1.725
B1/A0	-0.041	-0.005	0.218	-0.178	-0.258	-0.060
+-	0.144	0.140	0.152	0.176	0.163	0.185
B2/A0	-0.541	-0.460	-0.460	-0.043	-0.513	-0.579
+-	0.147	0.140	0.157	0.175	0.165	0.192
B3/A0	0.047	-0.023	0.043	-0.138	-0.250	-0.203
+-	0.135	0.128	0.142	0.154	0.153	0.178
B4/A0	-0.291	-0.158	-0.136	0.009	-0.331	-0.229
+-	0.118	0.109	0.124	0.137	0.138	0.157
B5/A0	0.064	-0.208	-0.076	0.164	-0.115	0.046
+-	0.107	0.096	0.112	0.118	0.125	0.140
B6/A0	-0.015	-0.007	0.055	-0.033	-0.046	-0.064
+-	0.098	0.089	0.100	0.112	0.115	0.129

cross section can be derived from isospin symmetry alone. The relation is:

$$\sigma(\bar{K}N \to \Lambda\pi\pi, I = 0) = 3\sigma(K^-p \to \Lambda\pi^+\pi^-) - 1.5\sigma(K^-n \to \Lambda\pi^-\pi^0).$$

Since we measured both cross sections appearing on the r.h.s., we present the result for the $I = 0$ cross section in fig. 14. The enhancement at $E^* \sim 1685$ MeV may be attributed to a $\Lambda(1690)$ and/or $\Lambda(1670)$. The directly measured (although statistically less significant) $I = 0$ cross sections $\sigma(K^-p \to \Lambda\pi^0\pi^0)$ from refs. [20,21] are compatible with our results.

5.4. *The* $\Sigma(1660)$ *resonance*

The formation of $\Sigma(1660)$ as seen in $(\Sigma\pi)^-$, $\Lambda\pi^-\pi^0$ and weakly in $\Sigma^-\pi^+\pi^-$ is characterized by the following observations:

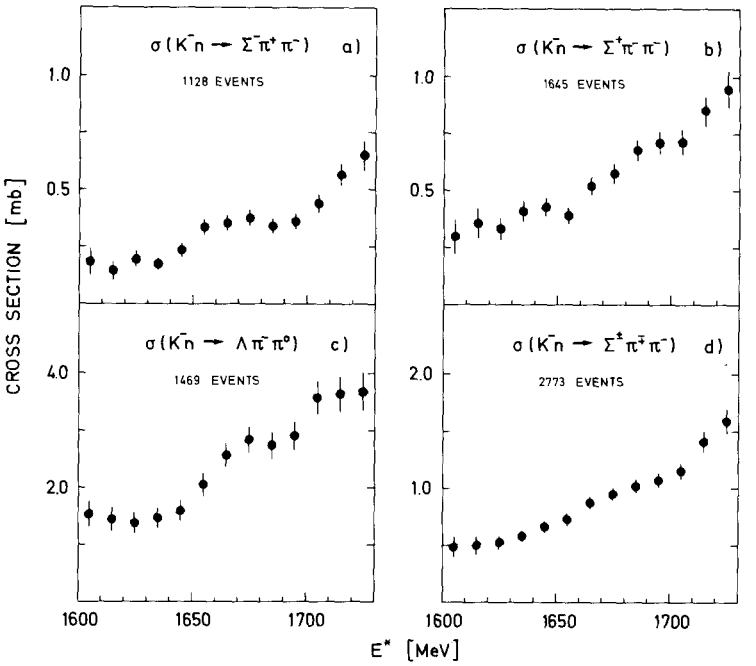

Fig. 8. Cross sections for the three-body reactions (4) to (6). The points in fig. 8d are the sum of the corresponding points in figs. 8a and 8b.

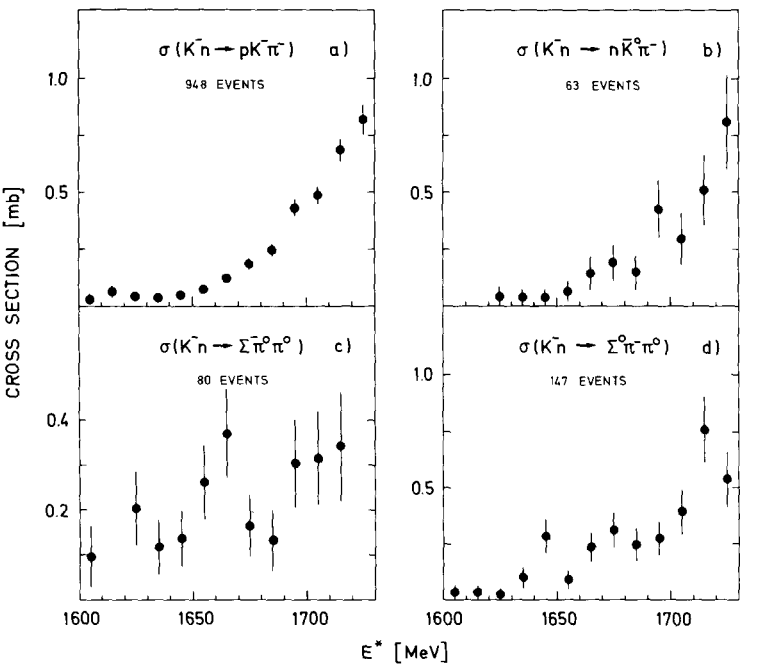

Fig. 9. Cross sections for the three-body reactions (7) to (10).

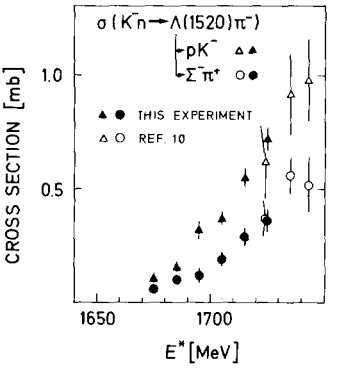

Fig. 10. Cross sections for the reactions $K^-n \to \Lambda(1520)\,\pi^- \to pK^-\pi^-$ (triangles) and $K^-n \to \Lambda(1520)\pi^- \to \Sigma^-\pi^+\pi^-$ (circles). The open triangles and circles represent twice the cross section for the corresponding reactions on protons [10].

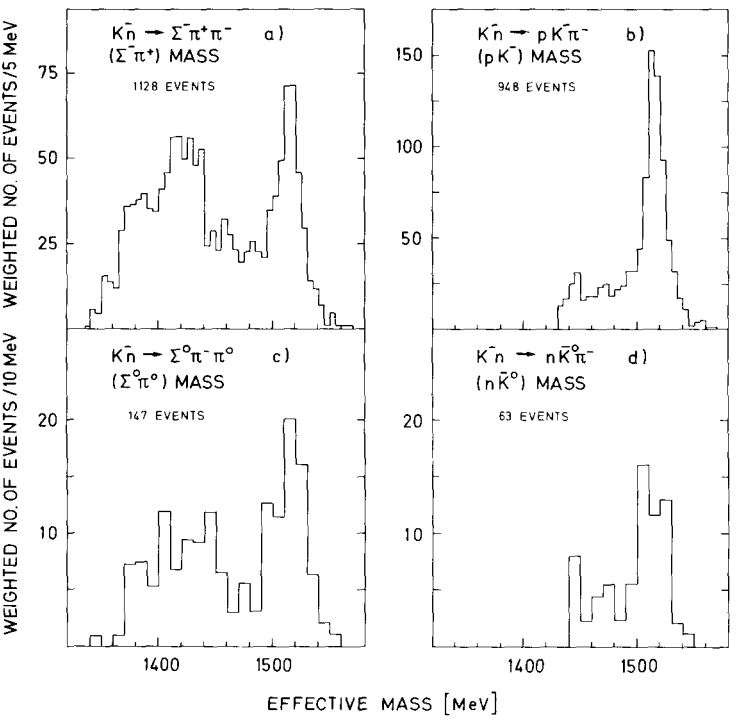

Fig. 11. Distribution of invariant masses: (a) $\Sigma^-\pi^+$ in the reaction $K^-n \to \Sigma^-\pi^+\pi^-$; (b) pK^- in the reaction $K^-n \to pK^-\pi^-$; (c) $\Sigma^0\pi^0$ in the reaction $K^-n \to \Sigma^0\pi^-\pi^0$; (d) $n\bar{K}^0$ in the reaction $K^-n \to n\bar{K}^0\pi^-$.

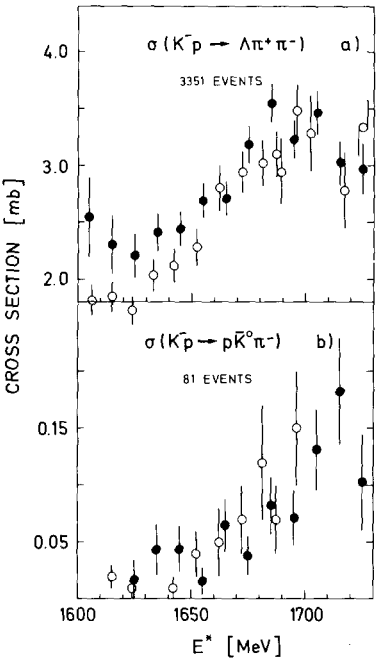

Fig. 12. Cross sections for K^-p reactions (full circles). The corresponding results obtained in hydrogen [7] are plotted as open circles.

(i) the enhancement is at $E^* \approx 1675 \pm 10$ MeV;

(ii) the branching ratio $\Sigma\pi\pi/\Sigma\pi$ is small ($\lesssim 0.2$ from this experiment).

Production experiments claim two resonant states in this energy region, both with masses of $M \approx 1660 \pm 3$ MeV [19]. One of these resonant states is produced with a large $\Sigma\pi\pi/\Sigma\pi$ branching fraction (~ 2) for small momentum transfers. Both resonances do not couple to $\bar{K}N$ ($<3\%$). On the other hand, all partial-wave analyses of formation experiments agree on an elasticity of about (0.10 ± 0.02) and claim masses around 1675 MeV. We conclude that the $\Sigma(1660)$ as seen in formation experiments is difficult to reconcile with either of the two resonances found in production experiments.

We are very much indebted to R. Armenteros, M. Ferro-Luzzi and P. Baillon for their continuous support and for numerous fruitful contributions in all stages of the experiment. We are grateful to N. Schmitz and K. Tittel for informative discussions and a critical reading of the manuscript. We wish to thank the crews of the proton synchrotron and the 81 cm bubble chamber for their participation in the exposure of this experiment and we acknowledge the continued efforts of our scanning and measuring staffs.

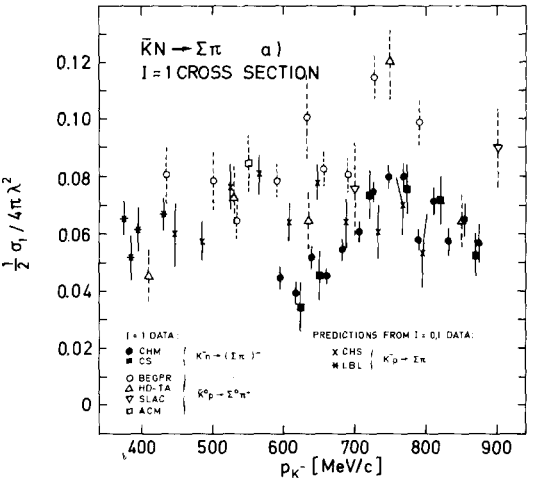

a

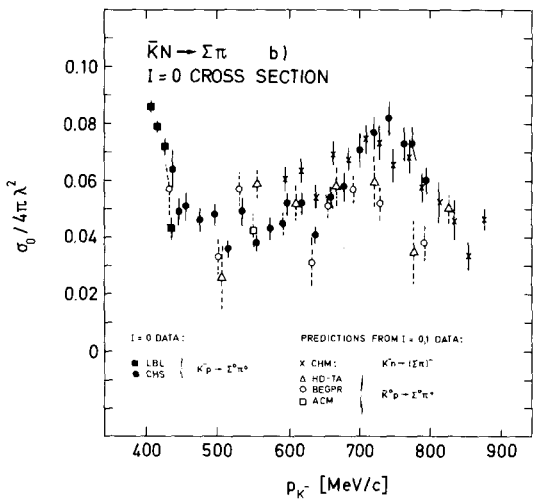

b

Fig. 13. Compilation of cross sections for $\bar{K}N \to \Sigma\pi$: (a) $\sigma(\bar{K}N \to \Sigma\pi, I = 1)/(8\pi\lambda^2)$; (b) $\sigma(\bar{K}N \to \Sigma\pi, I = 0)/(4\pi\lambda^2)$. The data were taken from the following references: CHM, this experiment; CS, [5, 12]; CHS, [7]; LBL [14]; BEGPR, [15]; HD-TA, [16]; SLAC, [17]; ACM, [18].

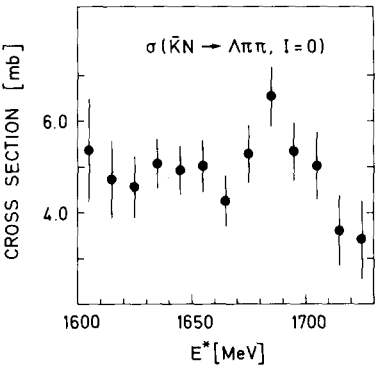

Fig. 14. The $I = 0$ cross section for $\bar{K}N \to \Lambda\pi\pi$ derived from $\sigma(K^-n \to \Lambda\pi^-\pi^0)$ and $\sigma(K^-p \to \Lambda\pi^+\pi^-)$ as measured in this experiment.

References

[1] D.E. Plane, Purdue Conf. 1973, MPI report MPI-PAE/Exp. El. 33;
G.P. Gopal, G.E. Kalmus, A.C. McPherson, R.T. Ross, A.J. Van Horn, T.C. Bacon, I. Butterworth and E.F. Clayton, Rutherford Laboratory report RL-75-182 (1976).

[2] Particle Data Group, N. Barash-Schmidt, A. Barbaro-Galtieri, C. Bricman, V. Chaloupka, D.M. Chew, R.L. Kelly, T.A. Lasinski, A. Rittenberg, M. Roos, A.H. Rosenfeld, P. Söding, T.G. Trippe and F. Uchiyama, Phys. Letters 50B (1974).

[3] R.V. Reid, Ann. of Phys. 50 (1968) 411.

[4] G. Alberi, L.P. Rosa and Z.D. Thomé, Phys. Rev. Letters 34 (1975) 503.

[5] R. Armenteros, P. Baillon, P. Lexa, A. Minten, K.H. Nguyen, E. Pagiola, V. Pelosi, R. Barloutaud, F. Bigata, M. Crozon, C. Louedec, J.L. Narjoux and F. Pierre, Nucl. Phys. B18 (1970) 425.

[6] R.J. Glauber, Phys. Rev. 100 (1955) 242;
V. Franco and R.J. Glauber, Phys. Rev. 142 (1966) 1195.

[7] R. Armenteros, M. Ferro-Luzzi, D.W.G.S. Leith, R. Levi-Setti, A. Minten, R.D. Tripp, H. Filthuth, V. Hepp, E. Kluge, H. Schneider, R. Barloutaud, P. Granet, J. Meyer and J.-P. Porte, Nucl. Phys. B8 (1968) 233;
R. Armenteros, P. Baillon, C. Bricman, M. Ferro-Luzzi, E. Pagiola, J.O. Petersen, D.E. Plane, N. Schmitz, E. Burkhardt, H. Filthuth, E. Kluge, H. Oberlack, R.R. Ross, R. Barloutaud, P. Granet, J. Meyer, J.P. Porte and J. Prevost, Nucl. Phys. B21 (1970) 15.

[8] R.D. Tripp, Ann. Rev. Nucl. Sci. 15 (1965) 325.

[9] B. Deler and G. Valladas, Nuovo Cimento 45A (1966) 559.

[10] E. Burkhardt, H. Filthuth, E. Kluge, H. Oberlack, R.R. Ross, B. Conforto, D.M. Harmsen, T. Lasinski, R. Levi Setti, M. Raymund, R. Armenteros, M. Ferro-Luzzi, D.W.G.S. Leith, A. Minten, R.D. Tripp, R. Barloutaud, P. Granet, J. Meyer and J.P. Porte, Nucl. Phys. B14 (1969) 106.

[11] G. Alberi, M.A. Gregorio and Z.D. Thomé, Nuovo Cimento 19A (1974) 585.

[12] R. Armenteros, P. Baillon, A. Minten, N.H. Khanh, V. Pelosi, M. Crozon, C. Louedec, J.L. Narjoux and F. Pierre, Nucl. Phys. B10 (1969) 459.

[13] J.H. Bartley, R.Y.L. Chu, R.M. Dowd, A.F. Greene, J. Schneps, W.H. Sims, J.R. Albright, E.B. Brucker, J.E. Lanutti, B.G. Reynolds, M. Meer, J.E. Müller, M. Schneeberger and S.E. Wolf, Phys. Rev. Letters 21 (1968) 1111.

[14] A. Barbaro-Galtieri, Int. Conf. on elementary particles, Lund, 1969;
R.D. Tripp, private communication.

[15] BEGPR-Collaboration: L. Bertanza, W. Cameron, P. Capiluppi, P. Croft, E. Flaminio, R. Jennings, G. Kalmus, P. Lugaresi-Serra, G. Mandrioli, A. Minguzzi-Ranzi, W. Morton, A. Nappi, R. Pazzi, K.J. Peach, A.M. Rossi, B. Saitta and W. Venus, Rutherford Laboratory report RL-76-016 (1976).

[16] E. Burkhardt, A. Pfeiffer, A. Putzer, G. Alexander, I. Bar-Nir, O. Benary, I. Borowitz, S. Dagan, A. Levy, D. Lissauer and Y. Oren, Nucl. Phys. B99 (1975) 365.

[17] R.J. Yamartino, G.W. Brandenburg, W.B. Johnson, D.W.G.S. Leith, J.S. Loos, G.J. Luste, J.A.J. Matthews, K. Moriyasu, W.M. Smart and F.C. Winkelmann, Phys. Rev. D10 (1974) 9.

[18] Y. Cho, M. Derrick, R.J. Miller, R.P. Smith, A. Engler, G. Keyes, R.W. Kraemer, J. Schlereth and M. Tanaka, Phys. Letters 60B (1976) 293.

[19] Amsterdam-CERN-Nijmegen-Oxford-Collaboration, Contribution to Int. Conf. on high-energy physics, Palermo, 1975;
S.P. Apsell, P. Ford, S. Gouveritch, L.E. Kirsch, P.E. Schmidt, P.Y. Chang, Stottlemyer, G.B. Yodh, S. Glickman, M. Goldberg, S.M. Jacobs, B. Meadows, G.C. Moneti, J. Brenner, J. Schneps and G. Wolsky, Phys. Rev. D10 (1974) 1419;
P. Eberhard, LBL report LBL-2012 (1973).

[20] T.Dombeck, W.W.M. Allison, J. Campbell, Y. Cho, M. Derrick, R. Engelmann, T. Groves, T.P. Wangler, N.S. Wong and D. Koetke, Phys. Rev. D7 (1973) 1331.

[21] R.Y.L. Chu, G.W. London, Y.P. Yu, D. Boyd, T. Beggs, D.J. Candlin, A.T. Goshaw, H.W.K. Hopkins, W. Venus, P. Alibran, S. Kahn, J.P. Lowys, R. Stump, J.P. Wuthrick, J. Colas, C. Farwell, A. Ferrer, E. Gombosi, T. Hofmokl, J. Six, D. Gamba, A. Marzari, A. Romero and A.E. Werbrouck, Nucl. Phys. B64 (1973) 109.